Bat Inspired Lifesize Ornithopter with Passive Lateral Wing Retraction

Logan Kelley

Thesis submitted to the Faculty of the

Virginia Polytechnic Institute and State University

in partial fulfillment of the requirements for the degree of

Masters of Science

in

Mechanical Engineering

Alexander Leonessa, Chair

Rolf Mueller

Kaveh Akbari Hamed

May 6, 2024

Blacksburg, Virginia

Keywords: Bat, Robot, Bio-Inspired, Lifesize, Ornithopter

Bat Inspired Lifesize Ornithopter with Passive Lateral Wing Retraction

Logan Kelley

ABSTRACT

Bats have a unique flying style that allows them to be highly dexterous in capturing prey and have great freedom of movement in flight. Bats' wings have a wing membrane that is tensioned by their fingers and arms, allowing them to retract their wings laterally in flight. This distinct motion has allowed bats to be the only mammals capable of sustained flight, adding to their evolutionary uniqueness.

This thesis presents the creation of the VALKRIE (Versatile Aerial Lifesize Kinetic Robot Inspired by bat Evolution) project: a to-scale simplified bat-inspired ornithopter that can be remotely controlled, sustain flight, and passively retract and extend its wings laterally. VALKRIE mimics the dimensions and size of its biological counterpart, *Hipposideros diadema*, a medium-sized bat; setting its aerodynamical constraints to the dimensions of *Hipposideros diadema*.

Bats' maneuverability is derived from their unique wing motion while in flight, retracting and extending their wings. VALKRIE mimics this motion by simplifying the joint structure of a bat's wing and passively retracting and extending the wings. By simplifying the complex anatomy of bat wing motion, VALKRIE can maintain flight and generate sufficient lift for increasing altitude. With a simplified design, VALKRIE only has two motors that actuate wing flapping, wing retraction, and rotation of the hind legs. With this simplified design, the operator can remotely control VALKRIE by increasing and decreasing the wingbeat frequency and steering to the right and left with the hind legs.

Acknowledgments

First, I would like to thank my fiancé, Lauren; she has given me the support and motivation that drives me to push myself to better myself and my education. Thank you to my parents; they have given me the support and resources to pursue what I want in life and for the morals that they have instilled upon me. Next, I would like to thank my advisor and mentor, Dr. Alexander Leonessa; he has given me the opportunity, guidance, advice, and environment required to create my project; he has pushed me in the right directions and guided me in directions I had yet to realize. Thank you to Jungsoo Park of the TREC lab; he started the robotic bat project in the TREC lab and has been invaluable in discussions and content knowledge. Lastly, I would like to thank the members of the TREC lab for their support and collaboration.

Contents

List of Figures

List of Tables

Chapter 1

Introduction

Bats are highly maneuverable and agile flying animals that have evolved for over 50 million years [1]. VALKRIE (Versatile Aeronautical Lifesize Kinetic Robot Inspired by bat Evolution) takes inspiration from bats by simplifying the complex anatomy of a bat's wing structure to create a controllable ornithopter capable of flight. There are over 1,000 bat species that vary in size, weight, and anatomy [2]. VALKRIE retains dimensions and wing structure similar to *Hipposideros diadema* (Diadem leaf-nosed bat), a bat with a medium-sized wingspan of up to 54 cm [3].

Flying robots of smaller sizes are denoted as mini-Unmanned Aerial Vehicles (UAVs), with the largest dimension of the aircraft being between 50 cm and 200 cm [4]. Mini-UAV applications are vast and include surveillance, reconnaissance, communications, environmental monitoring, and even parcel delivery. Research groups, private companies, and the military have all created biology-inspired bat robots to accomplish one of the applications of mini-UAVs [5][6][7].

VALKRIE is not the first biology-inspired robot; in fact, several attempts have been made to create a life-size model of medium-sized bats: B2, BATMAV, and BatBot [6][8][9]. The medium-sized robotic bat projects mimic the wing retraction and size of medium-sized bats but are incapable of sustained slight.

There has been two bat-inspired ornithopters that have successfully sustained flight but have large wingspans of 228 cm and 168 cm; comparing to only one species of bat, the giant golden-crowned flying fox (*Acerodon jubatus*), which has a wingspan of 150 cm [10][11][12]. These flying fox inspired robots are not scalable to other size bats and fail to mimic the high maneuverability and smaller size of most bats.

The two bat inspired ornithopters capable of flight are the Festo Flying Fox and the Beihang University ornithopter as shown in Figure 1.1. The Festo Flying Fox has a wingspan of 228cm, which is outside the wingspan range of the largest known bat, and neither the Beihang University ornithopter nor Festo Flying Fox has the lateral wing retraction of bats, a defining characteristic of bats' flying motion.

This makes VALKRIE the first robotic bat with a wingspan of less than 100cm and the capability to increase and maintain altitude in flight. In addition, VALKRIE is the lightest of the biology-inspired bat robots while maintaining remote controllability. Some of the bat-inspired robots contain the ability to extend and retract their wings, but all do so actively. VALKRIE is the only biology-inspired robot with passive lateral wing retraction, making it the first to-scale medium-sized biology-inspired robot to maintain flight and the first ornithopter to have passive lateral wing retraction.

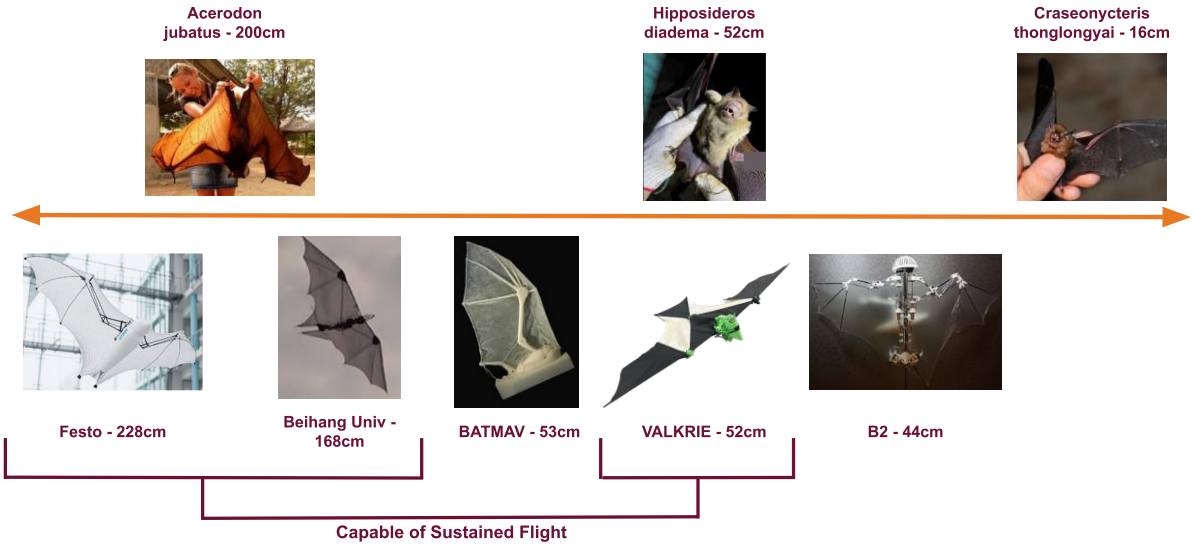

Figure 1.1: Size Chart of Bats and Robotic Bats [5][13][11][8][14][6][15]

1.1 Outline

VALKRIE is a complex system reaching across multiple fields: biology, aerodynamics, mechanical design, electrical design, and computer science. VALKRIE takes inspiration from its biological counterpart's dimensions, shape, and flying motion. Flying parameters were inspired by bats, such as wingbeat frequency, wing amplitude, wing retraction, and wing weight to total weight ratio. This project depended on reliable mechanical design in the wing retraction mechanism, wing driving mechanism, and chassis to hold everything together. VALKRIE has many electrical components to drive the wings, hindlegs, and controls. To match the hardware, software was implemented to receive inputs, process the inputs, and send outputs so VALKRIE could fly and be operated by a remote user. Many variations and combinations of potential solutions have been built and tested for VALKRIE. Multiple mechanical designs, motors, wing membranes, and concepts have led to the current version of VALKRIE's ability to fly.

There are many aspects that VALKRIE is comprised of such as biological, mechanical, electrical, and software components. The following chapters organize this thesis to present the creation and evaluation of VALKRIE:

Chapter 2 is about biological inspiration. By analyzing the flying motion of bats, VALKRIE can utilize parameters and concepts that will allow for successful flight. VALKRIE seeks to mimic the complex flying motion of bats and the dimensions and parameters of a medium-sized bat, *Hipposideros diadema*.

Chapter 3 covers the mechanical design of VALKRIE. This chapter discusses previous iterations and ideas that led to the current design of VALKRIE. This section explains the different mechanical components of VALKRIE and their functionality. This chapter also describes the wing retraction design and how the wing retraction can be calculated and evaluated.

Chapter 4 descirbes the electric components of VALKRIE. This chapter evaluates different electrical components from previous iterations. This section considers the various electronic components, their function, and their contribution to flight and control.

Chapter 5 covers the software that enables VALKRIE to fly. This chapter explains the code that is implemented with VALKRIE. The software is responsible for receiving inputs and calculating the outputs to the motors so that VALKRIE can maintain a stable flight.

Chapter 6 details the assembly of VALKRIE. With every part manufactured and chosen, VALKRIE can be fully assembled. This section described the building process and how each part came together to create the final version of VALKRIE.

Chapter 7 reports on the testing of VALKRIE. It presents the processes and data collection from testing the final version of VALKRIE. This chapter also presents data showing how long and far VALKRIE can fly and loading tests.

Chapter 8 presents the conclusions based on the analysis of VALKRIE. With all of the data presented and evaluated, VALKRIE is shown to be a successful biology-inspired robot that mimics *Hipposideros diadema*. This section also explores the future work and potential of VALKRIE.

Chapter 2

Biology

Understanding the biology that inspired VALKRIE is key to understanding the design decisions that created VALKRIE. As a bat inspired robot, many of the design decisions and concepts come from the biology of bats. The complex flying motion of bats can be broken down into several different sections, such as the mechanics of bats' wing structure, the wing membrane, wing retraction, and the size and weight of VALKRIE's biological counterpart, *Hipposideros diadema*. Through understanding the structure and concepts of the flight of bats, VALKRIE can utilize the successful model of bats to gain the ability to sustain flight.

2.1 Bat Wing Mechanics

To achieve efficient flight, bats have evolved a complex biological wing structure of 25 active joints per wing [16]. Bats have a distinct way of flying that differs from birds and insects; the image below compares the bone structure of bats to that of humans and birds, as shown in Figure 2.1 [17]. As mammals, bats do not have feathers; bats have a living skin membrane that attaches to their fingers, arms, body, and hind legs. Bats' skin can stretch, allowing them to move their limbs in flight. Bat membranes must stretch to retract their wings while maintaining tension in their wing membrane. Tension in the membrane is vital to generating lift and maintaining flight [18].

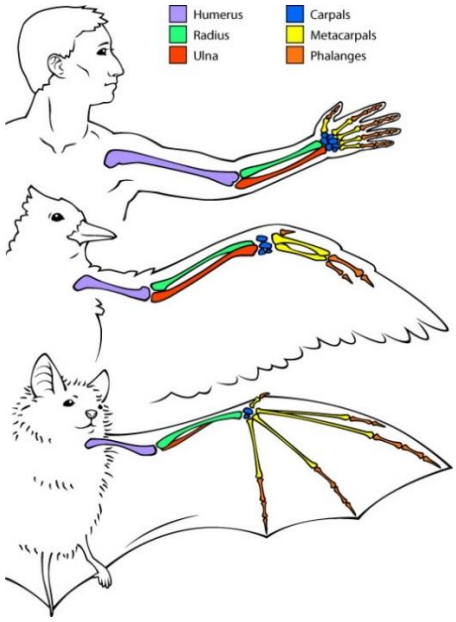

Figure 2.1: Bat Wing Anatomy Comparison [17]

Bats are the only living animals that use a membrane for flight. The largest flying animals to have ever existed are the pterosaurs, with wingspans of up to 11 meters [19]. A pterosaur wing is much like a bat's wing in that both animals use a wing membrane, but pterosaurs only use one finger for the structure of the wing membrane, whereas bats use four fingers to structure the wing membrane and offer maneuverability. The structure of a wing membrane is present in the largest of all flying animals and in the smallest known mammals. The maneuverability and vast size range in flying membrane animals shows the broad effectiveness of a wing membrane structure. Millions of years after the pterosaurs became extinct, bats have evolved a similar wing structure to that of a pterosaur through convergent evolution.

One of the benefits of having a wing membrane compared to feathers is that it creates a steeper lift slope and larger lift coefficients compared to birds' wings [20]. Other benefits include easy retraction of the wing and altering the wing structure with the hind legs and the many joints in the fingers and arms.

A wing membrane allows for simple retraction while maintaining tension in the wing membrane. One of the main reasons bats can fly effectively is because bats retract their wings towards their body during upstroke and extend their wings during downstroke [21]. Retracting their wings during upstroke causes less negative lift; this increases the net lift per stroke of the wing. VALKRIE aims to mimic this behavior by retracting its wings towards the body during the upstroke and extending the wing during the downstroke. Figure 2.2 shows the main joints on a bat wing and how they rotate towards and away from the body.

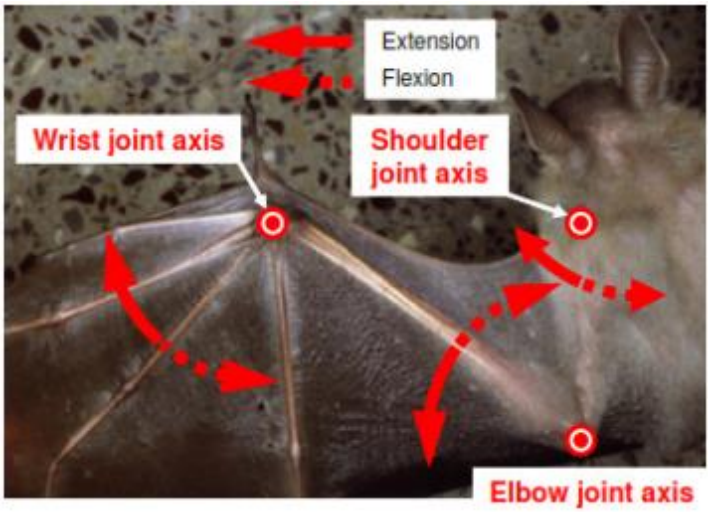

Figure 2.2: Bat Joint Rotation [22]

2.2 Hipposideros diadema

VALKRIE's dimensions were based on *Hipposideros diadema*, shown in Figure 2.3. *Hipposideros diadema* is a bat that eats insects while in the air and is considered a narrow space forager [23]. This medium-sized bat was chosen for its maneuverability, size, and available data.

This maneuverable bat has a wingspan of up to 54.3 cm and an average weight of 46.9 grams [3] [25]. The head and body length of *Hipposideros diadema* is 19 cm, as shown in Figure 2.4 [14].

Figure 2.3: *Hipposideros diadema* [24]

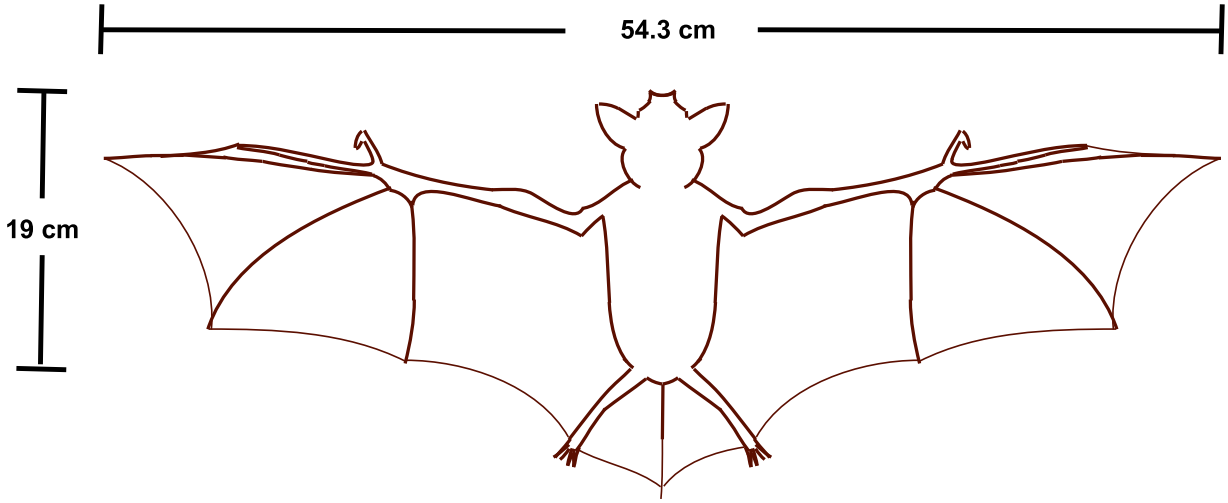

Figure 2.4: *Hipposideros diadema* Dimensions

The wingbeat frequency is a parameter of *Hipposideros diadema* the author could not directly find. Research has found a relationship between the bat's weight and the species' wingbeat frequency; there are two separate equations depending on the diet [26]. The wingbeat frequency equation for the insect-eating bats is shown in Equ. (2.1), this equation has an accuracy of ± 1 Hz [26].

$$f = 3.65 - 3.312 * \log_{10} m \qquad (2.1)$$

The estimated *Hipposideros diadema* wingbeat frequency from the equation is 8.05 Hz. The other parameter the author could not find for *Hipposideros diadema* is the wingbeat amplitude. Wingbeat amplitudes for bats can range from 50 to 100 degrees [26]. Splitting the difference between the extremes leads to a flapping amplitude of 75 degrees for mimicking a medium-sized bat.

2.3 Bat Wing Membrane

The wing membrane for bats is a thin skin with muscles. Generating the lift required for bats to fly, the wing muscles act as springs in flight [27]. This tension in the wing allows for the wings to push down on the air, creating lift and thrust. Bat wing membranes are made of thin skin that is anisotropic across its area meaning the mechanical properties are not the same in all directions. The anisotropic skin allows for more strength along the direction parallel to the body; this allows the wing to stretch laterally for wing retraction, as shown in Figure 2.5 [28]. One of the main differences between a bat's wing and a bird's, besides the wing material, is how the wing membrane connects to the hind legs; this allows the legs to tension the wings and create complex and moving wing geometry for the bat in flight.

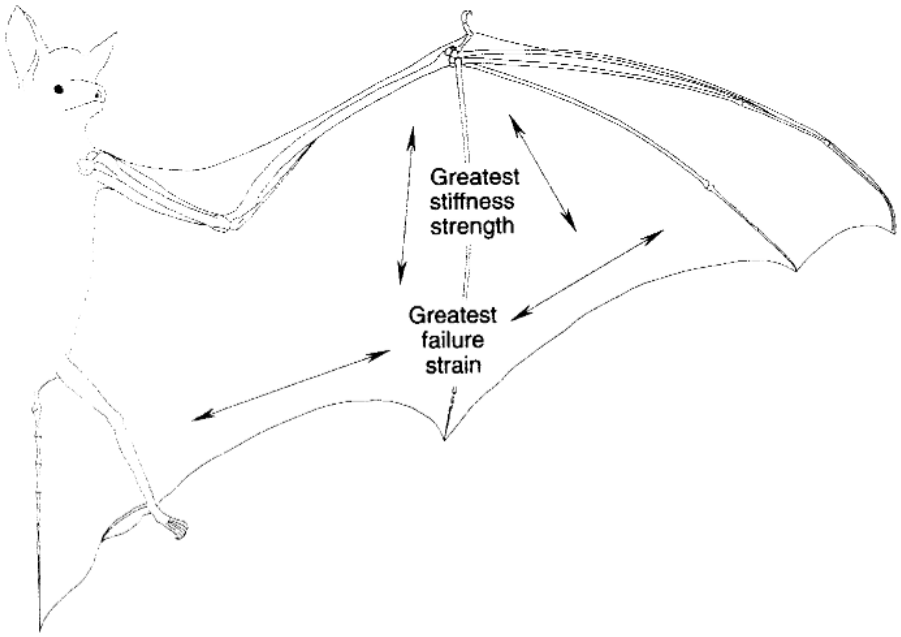

Figure 2.5: Anisotropic Mechanical Properties of Bat Wings [28]

2.4 Bat Wing Weight

The wing membrane attributes weight to the total weight of the wing. A study found a correlation between the wing's mass and the bats' total body mass, as shown in Equ. (2.2) where m_w mass of the wing (kg) and m_{tot} is the total mass of the bat in kg [29].

$$m_w = 0.112 {m_{tot}}^{1.11} \qquad (2.2)$$

The mass of the wing compared to the total weight of the bat is an important concept that affects inertial loss for flapping the wings. Bats are found to lose 18% of power due to the inertial power requirements of the wing **Error! Reference source not found.**. The relationship between the mass of the wing and the total mass is an important property to consider when mimicking bats.

2.5 Bat Wing Flight Motion

While the mass of the wings is essential to the motion of the bats, aerodynamic parameters that change in flight have been experimentally determined. The pitch and wingbeat frequency parameters have direct relationships to the lift and drag, and can be used to quantify the motion of bats.

2.5.1 Change in Pitch During Wing Stroke

Experimental data for pitch angle has been taken on a bat of the same family of *Hipposideros diadema*: *Hipposideros pratti*; this data is shown in Figure 2.6 [31]. Changing the pitch of the wings also changes the angle of attack for the wings. The angle of attack is the angle at which the wing area faces the airflow. As the angle of attack changes, the lift and drag change.

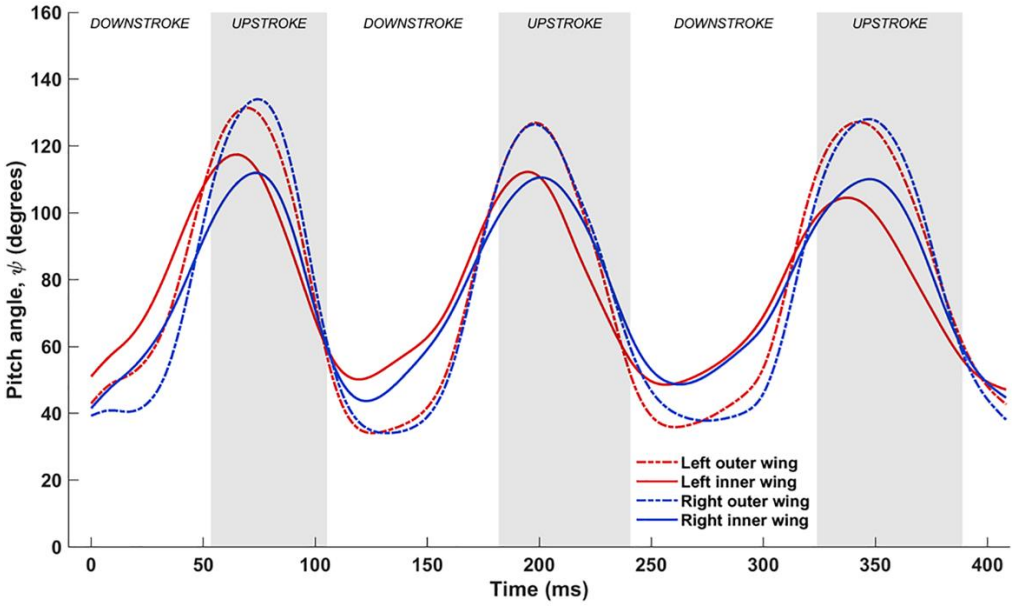

Figure 2.6: Pitch Variation of *Hipposideros pratti* in Flight [31]

The data shown in Figure 2.6 also indicates that the time it takes to produce a downstroke is larger than the time it takes for the bat to produce an upstroke [31]. The pitch and the difference in time to generate an upstroke versus a downstroke are defining characteristics of bats' flight that should be incorporated when mimicking the motion of a bat in flight.

2.5.2 Wingbeat Frequency in Flight

Bats fly at different wingbeat frequencies to achieve different motions. The wingbeat frequency can significantly affect the net lift created by the wings. A research paper determined the relationship between the wingbeat frequency of a biology-inspired robotic bat and the lift, as shown in Figure 2.7 [16]. The paper found that as the wingbeat frequency increases, the net lift increases. While VALKRIE has a desired wingbeat frequency to match

that of *Hipposideros diadema*, having an increased wingbeat frequency will generate more overall lift.

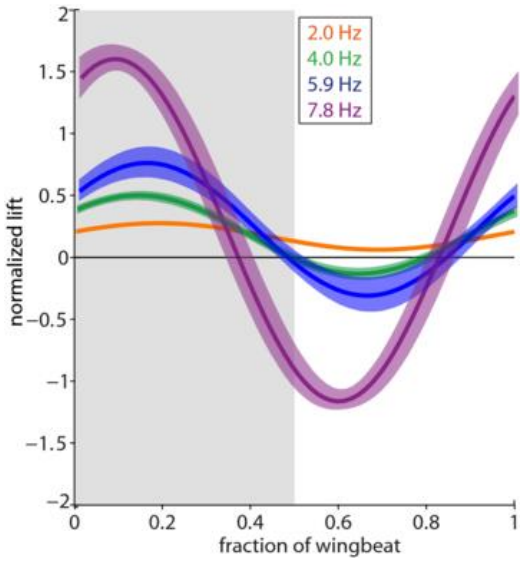

Figure 2.7: Wingbeat Frequency and Normalized Lift [16]

2.6 Biology Inspiration Overview

Overall, VALKRIE seeks to mimic many aspects of bats. The complex motion of bats can be broken down into several parameters and functionalities. VALKRIE mimics the parameters of wingspan, head to body length, wingbeat frequency, and wing weight to total weight ratio. Incorporating wing retraction, a wing membrane, a sinusoidal change in pitch motion, and the concept of having an upstroke taking less time than a downstroke are all concepts that VALKRIE seeks to mimic through the mechanical design described in the next chapter.

Chapter 3

Mechanical Design

There are several ways to translate the motion and parameters of bats to create a bat-inspired robot. Through the design process, there have been multiple iterations of VALKRIE to build a bat-inspired robot. This chapter will discuss previous iterations of VALKRIE and the design changes and decisions that created the latest version of VALKRIE. The mechanical design can be broken up into several subcomponents, including the body, the hind legs, the wings, the wing retraction, the wingbeat mechanism, and the wing material. Once the subcomponents were designed, most parts were created using additive manufacturing. After the pieces were manufactured, the total design could be tested by analyzing the weight, center of mass, change in pitch, lateral stability, and the passive wing retraction design area calculations.

3.1 Past Iterations

3.1.1 First VALKRIE

The first iteration of VALKRIE had over 186 parts. The latest design of VALKRIE has only 54 pieces. This drastic change in part numbers can be attributed to design simplification, part consolidation, and material selection.

This early design was a project of the TREC (Terrestrial Robotics Engineering & Controls) Lab at Virginia Tech and led by Jungsoo Park. This design used a brushless DC motor and printed gearbox to drive the wingbeat and wing retraction motion—the frame of this used laser cut fiberglass plate to hold the pieces together. When tested, the fiberglass would crack and eventually lead to propagation and shattering of the frame. For this reason, the next iteration would use a frame printed with PLA. Another point of failure for this design was the cam that drives the wing retraction and flapping motion. When the wingbeat frequency was increased enough, the cam would strip and no longer rotate. After sufficient use, the printed

gear teeth would be worn down. Because of the issues with the cam and printed gears, the next iteration of VALKRIE would implement a brushed DC motor with an attached metal gearbox that could withstand the stress experienced during flight.

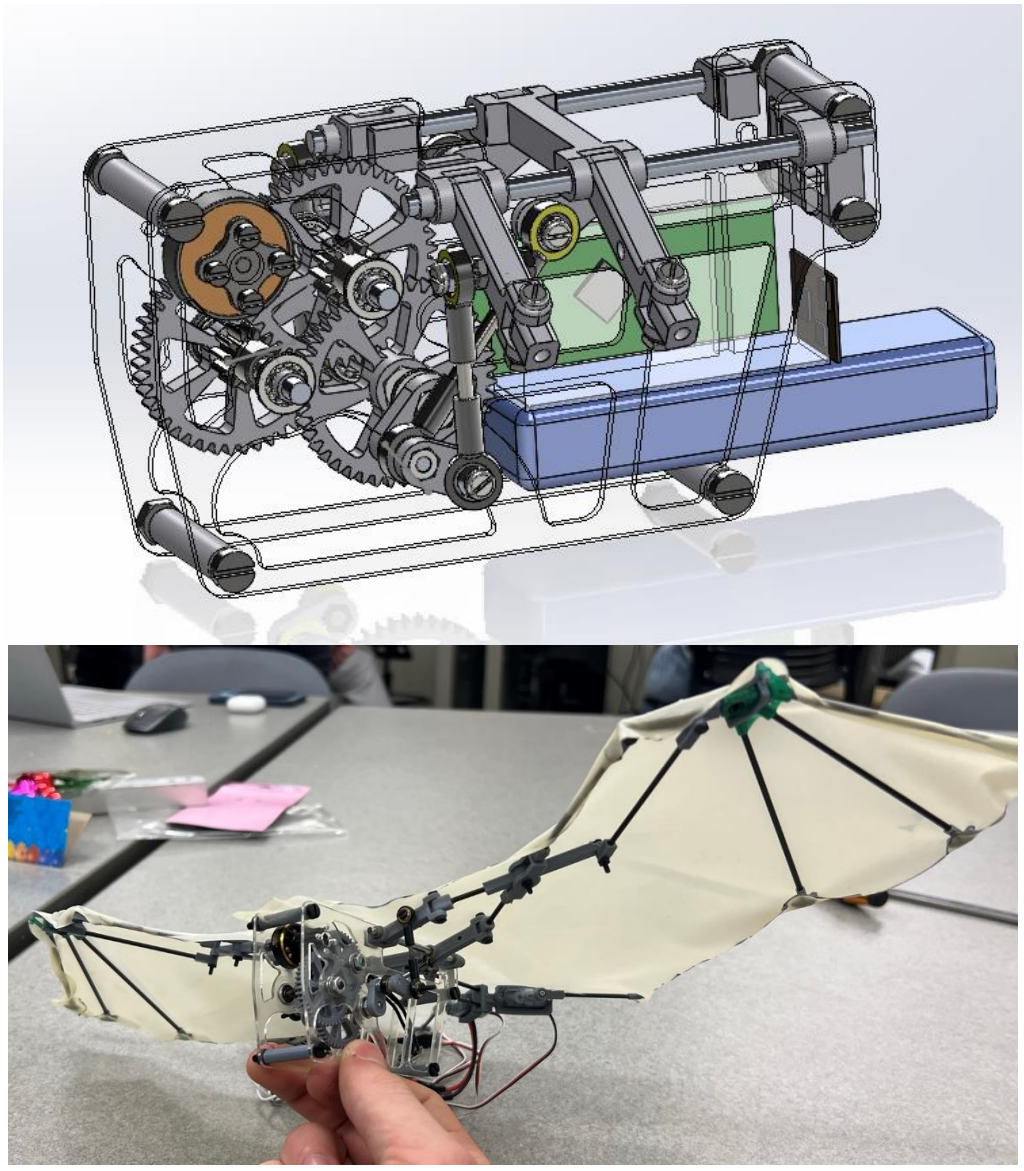

Figure 3.1: Early Design CAD and Build

3.1.2 Active Angle of Attack

After initial testing of the previous design, the author became the lead on the VALKRIE project, designing all further iterations and changes. The first design created by the author is the active angle of attack model. The active angle of attack design translates the motion from the driving motor to a shaft that moves the angle of the wings, with respect to the body, up and down, as shown in Figure 3.2. This design has more direct control over the wings' angle of attack but adds additional weight and complexity to the wing's structure. To translate this motion, a timing pulley was used. The timing pulley would often slip, causing the wing retraction to become out of phase. This design moved away from a printed gearbox and used a brushed DC motor with an attached metal gearbox for the driving motor.

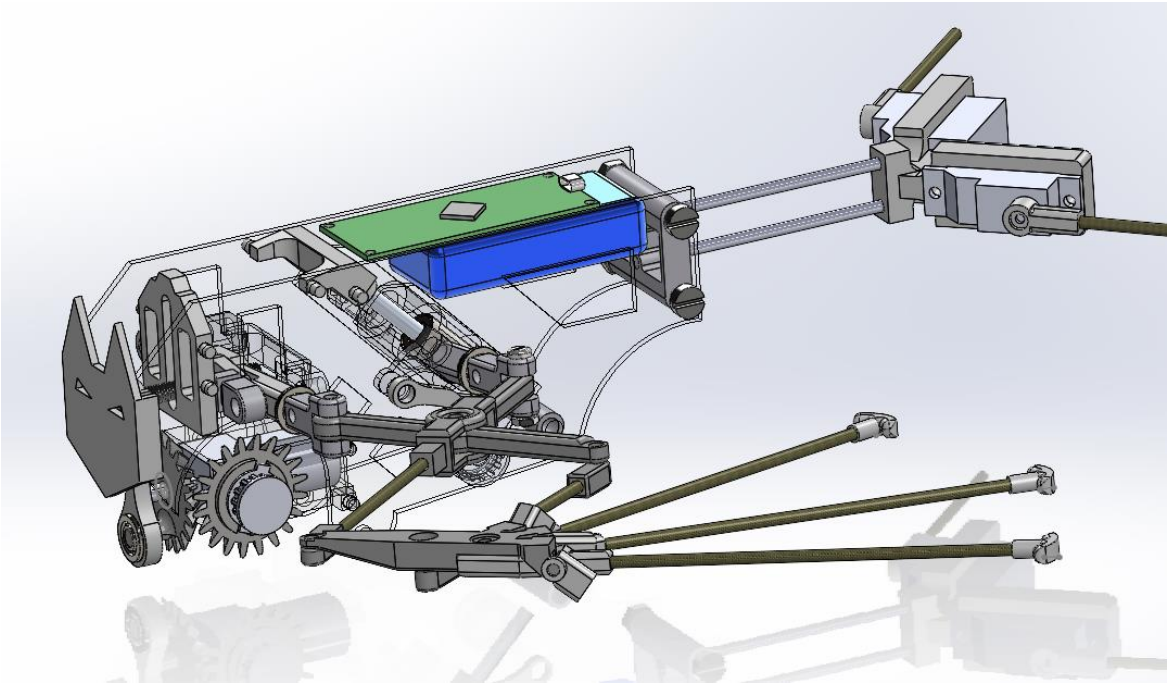

Figure 3.2: Active Angle of Attack CAD

3.1.3 Further Simplification

Perhaps one of the most significant leaps in design was to consolidate many parts of the body into a single part. This reduced the weight, number of parts, and assembly time. This design translates the motion of the driving motor to the angle of attack and wing retraction shaft; three gears were used. Each gear increased not only the weight but also the friction of the

system. The angle of attack design also required rotating joints to be added to the shoulders, adding more friction to the system. The increased friction and loading on the driving motor meant that even when over-voltaged, the wingbeat frequency only reached 8 Hz in flight. Due to these issues, VALKRIE was redesigned to have a less complex wing structure and wing retraction mechanism. The hind legs were also simplified into one servo to further decrease weight.

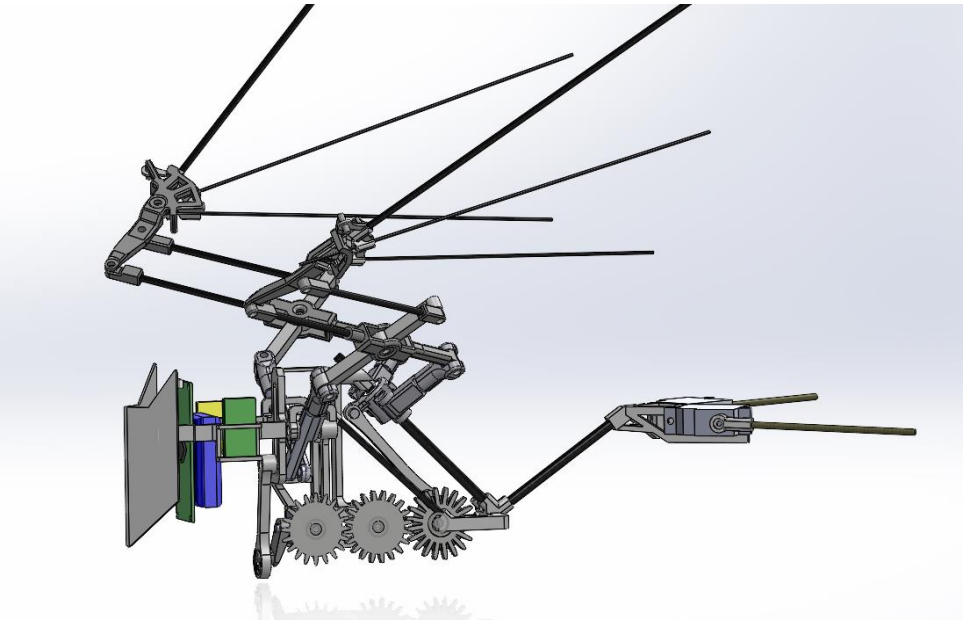

Figure 3.3: Part Consolidation CAD

3.2 Wing Retraction Mechanism

Unlike the previous models, the latest iteration of VALKRIE mimics the wing retraction of bats in flight using a passive wing retraction mechanism that folds the wings laterally. This design is not only unlike other iterations of VALKRIE but also unlike other bat-inspired robots. The wing retraction of the previous bat-inspired ornithopters with the ability for lateral wing retraction all have a similar wing retraction device, as shown in Figure 3.4 (a), (b). This series of linkages, which was also implemented in previous iterations of VALKRIE, shown in Figure 4.6 (c), actively extends and retracts the wings. This design contains many more mechanical joints and an overall increased loading on the motor. In addition to the increased loading on the motor due to friction, these designs weighed more than the passive wing retraction device of VALKRIE.

(a) Festo Flying Fox [5] (b) B2 [6] (c) Early VALKRIE Design

Figure 3.4: Wing Retraction Mechanisms

Some ornithopters use passive wing retraction, utilizing gravity to bend the wings down but not laterally like a bat [4]. The novel design of VALKRIE's wing retraction simplifies the process by using a tensioning mechanism that retracts the wings during upstroke and extends the wings during downstroke. This design is lightweight, using an 8-pound fishing line to retract the wing, as portrayed in Figure 3.5 (a) (b).

(a) (b)

Figure 3.5: Wing Retraction Mechanism in Tension

The wing retraction mechanism for VALKRIE has four parts. There is a fishing line, arm connector, finger connector, and a flexible material tensioner. Figure 3.6 illustrates the two connectors. The arm connector mounts to a 3mm hollow carbon fiber rod and is also an anchor point for the wing support rod. The finger connector mounts all the fingers and an anchor point for the fishing line to anchor. When in tension, the finger connector rotates around the arm connector, causing the wing's retraction.

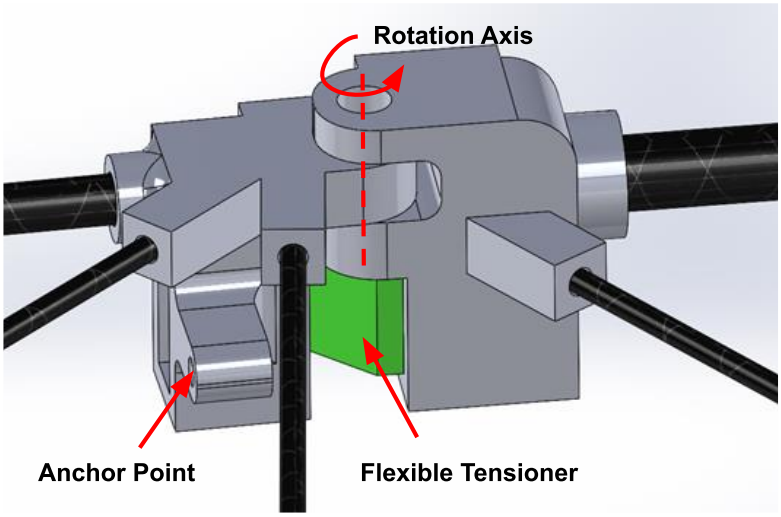

Figure 3.6: Wing Retraction Connectors

The flexible material tensioner is responsible for passively pulling the finger connector forward. TPU was used for the tensioner due to its elastic material properties. The flexible material is printed at a 90-degree angle, as shown in Figure 4.8, to ensure that tension is always pulling the fingers forward until they are parallel with the arm rod. The flexible material's width and thickness determine the line's tension. When there is not enough tension, the wing won’t extend; with too much tension, the motor will experience more torque than necessary. These dimensions were iterated so that the wing could extend without tension on the fishing line.

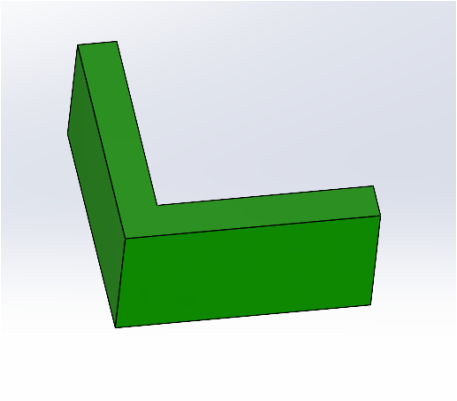

Figure 3.7: Flexible Material Tensioner

3.3 Wing Design

The design of the wing was created to mimic the wing profile of a bat. The wing profile has three fingers to represent a bat's last three metacarpals and phalanges, as shown in Figure 3.8. The leading finger is a hollow 2mm carbon fiber rod; the other two are made from a 1mm carbon fiber rod. The wing profile also simplifies the ulna and humerus into a single 3mm hollow carbon fiber rod that acts as the arm and attaches to the wingbeat mechanism. As the wings supply rigidity to the wing membrane for the outer wing, an additional support is used to create rigidity for the inner wing. The support for the inner wing is not inspired by bats but compensates for the lack of tension in the inner wing area. Where bats can create tension in the inner part of the wing with muscles, the support rod can create tension in the wing for VALKRIE.

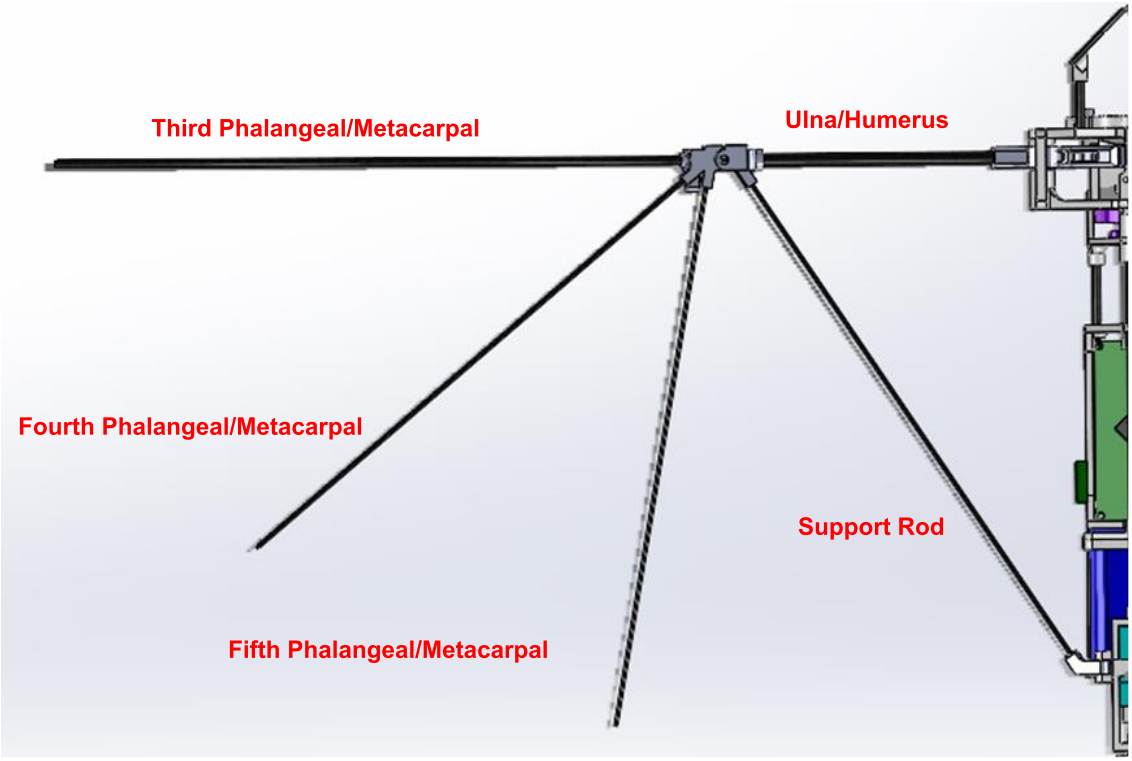

Figure 3.8: Wing Design

3.4 Wing Membrane Synthesis

With the various attempted bat-inspired robots, there have been several concepts for the wing membrane, as shown in Figure 3.9. Most robotic bats use a single isotropic material, such as the Festo Bionic FlyingFox and B2; they use a crystal membrane and silicone membrane, respectively [5][6]. There has been an attempt to mimic the anisotropic behavior of bat wings using elastic chords, as shown in Figure 3.9 (c), but it proved ineffective [9].

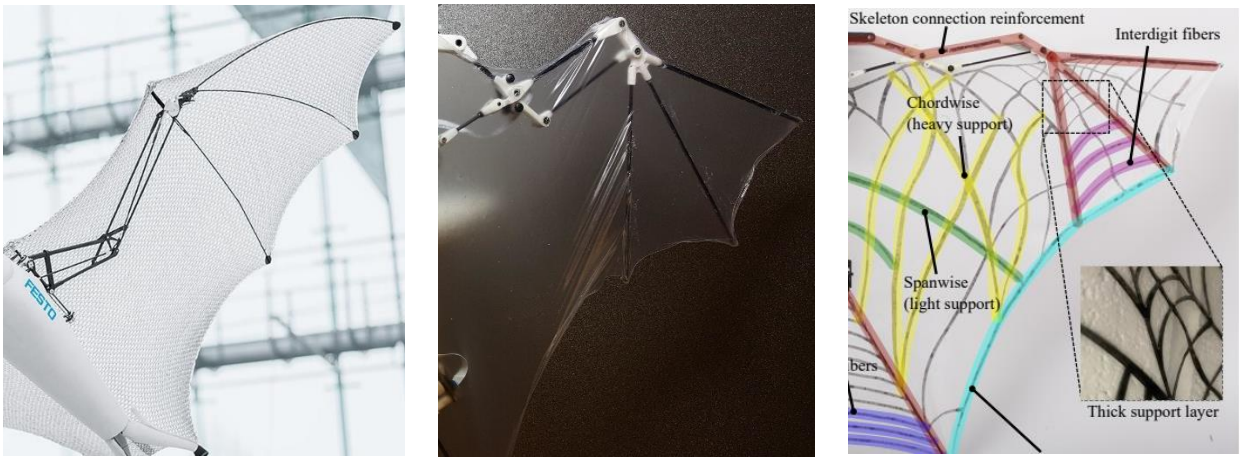

(a) [5] (b) [6] (c) [9]

Figure 3.9: Wing Membrane of Bat-Inspired Robots

Multiple wing membranes were considered and tested for VALKRIE. Both elastic and non-elastic materials were evaluated. The more elastic membrane materials considered were silicone rubber and natural rubber sheets. While these materials stretch similar to bat wings, they are not anisotropic, and the torque required to keep the wings in tension when extending the wing can decrease the speed of the driving motor.

The non-elastic wing membrane materials considered were a thin corrugated low-density polyethylene sheet, wear-resistant nylon film, and ripstop nylon. These materials deform less in flight and create a more stable flight; they also weigh less than their elastic counterparts.

VALKRIE combines an elastic and a non-elastic wing material for the wing membrane. VALKRIE uses non-elastic ripstop nylon where there is not a significant amount of deflection and utilizes the elastic natural rubber material where there is substantial deflection from the wings to the hind leg, as shown in Figure 3.10. The bi-material membrane offers rigidity for the wings and elasticity where bats' wings deflect the most, keeping tension in those areas.

Figure 3.10: Bi-material Wing Membrane

3.5 Driving Wingbeat Mechanism

The driving wingbeat mechanism is comprised of twelve parts. There are a total of five rotating axes for the driving mechanism, as shown in Figure 3.11. The motor rotates a series of two linkages that drive one of the shoulders up and down in a sinusoidal motion. The gear teeth on one shoulder then transfer the opposite motion to the other shoulder. This mechanism has six ball bearings to reduce the friction at each rotating axis except for the motor axis. Another mechanism developed used a series of three slots to drive the flapping motion: one slot on the body and a slot on each of the shoulders. The slotted design experiences more friction than the geared design, which is why the gear design was chosen.

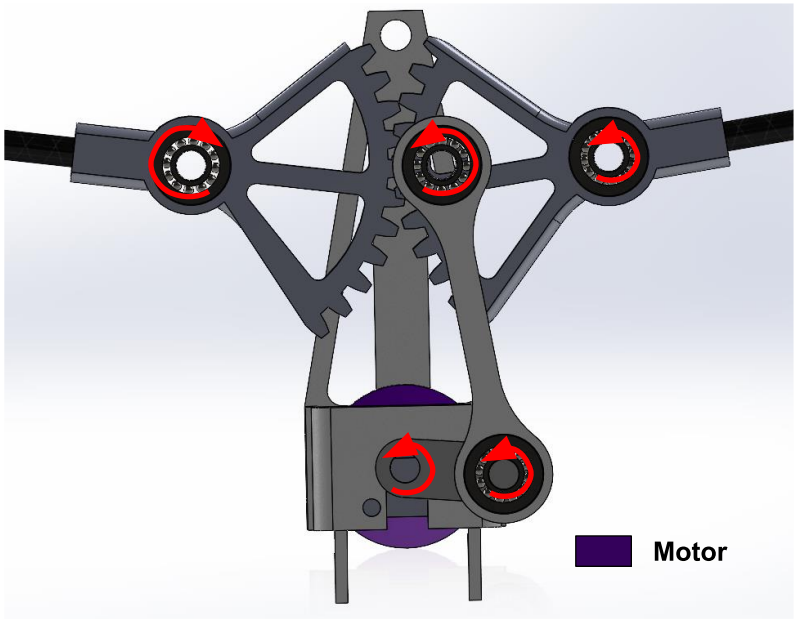

Figure 3.11: Wingbeat Mechanism

3.6 Body

The body mounts the wings, hind legs, and electronic components together. The body has a total of five parts, as shown in Figure 3.12. There are two printed parts for the body and three carbon fiber rods that connect the parts. The spine of the body is a 3mm hollow carbon fiber rod with a wall thickness of 0.5mm; this provides rigidity along the length of the body. This simplifies the complex anatomy of a bat's vertebrae and reduces the degrees of freedom for the spine. The two carbon fiber supports on the bottom of the body prevent the electronic chassis from deflection.

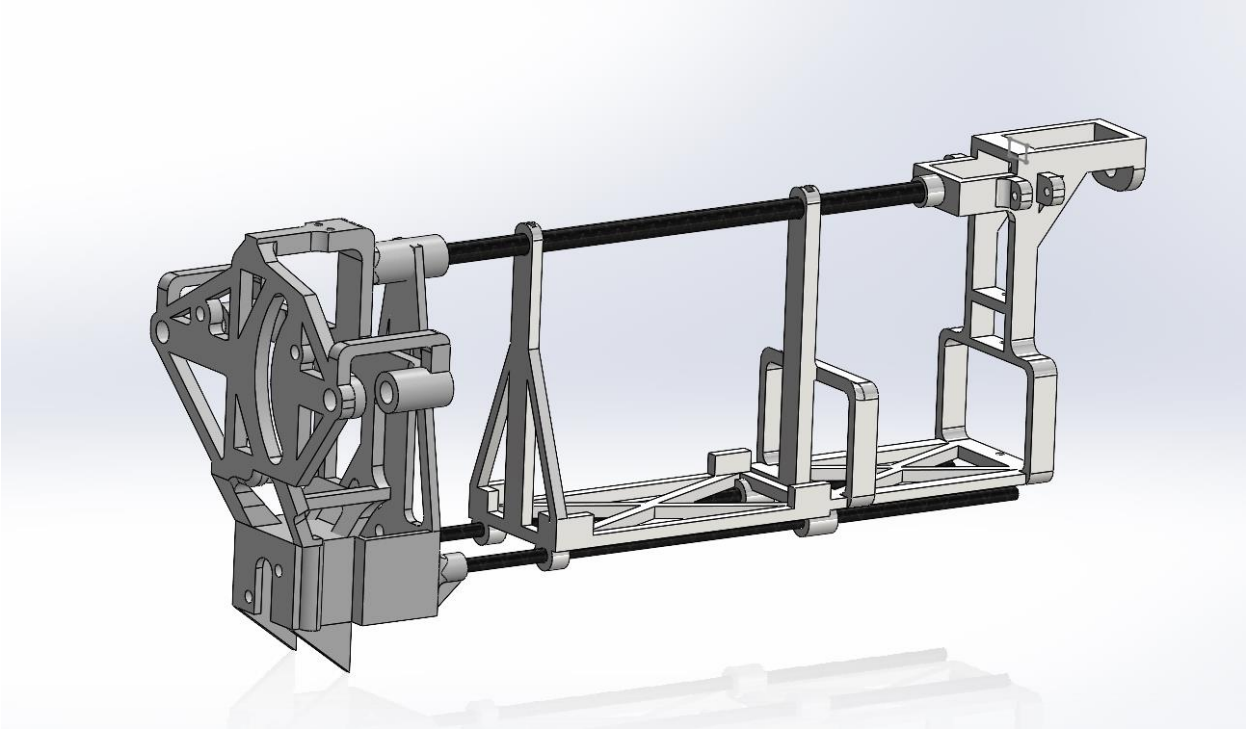

Figure 3.12: CAD of Body Components

3.7 Hind Legs

The hind legs of VALKRIE represent a simplified model of the hind legs of a bat, as shown in Figure 3.13. Controlled by a single servo, the coupled hind legs rotate together to steer the bat and control the roll. The hind legs are mounted to the body frame with a ball bearing to prevent a moment around the lateral direction onto the servo. Previous iterations had the hind legs directly mounted to the servo; during flight, the hind legs would break off the servo; thus, the design to attach the legs to the body with a ball bearing was created.

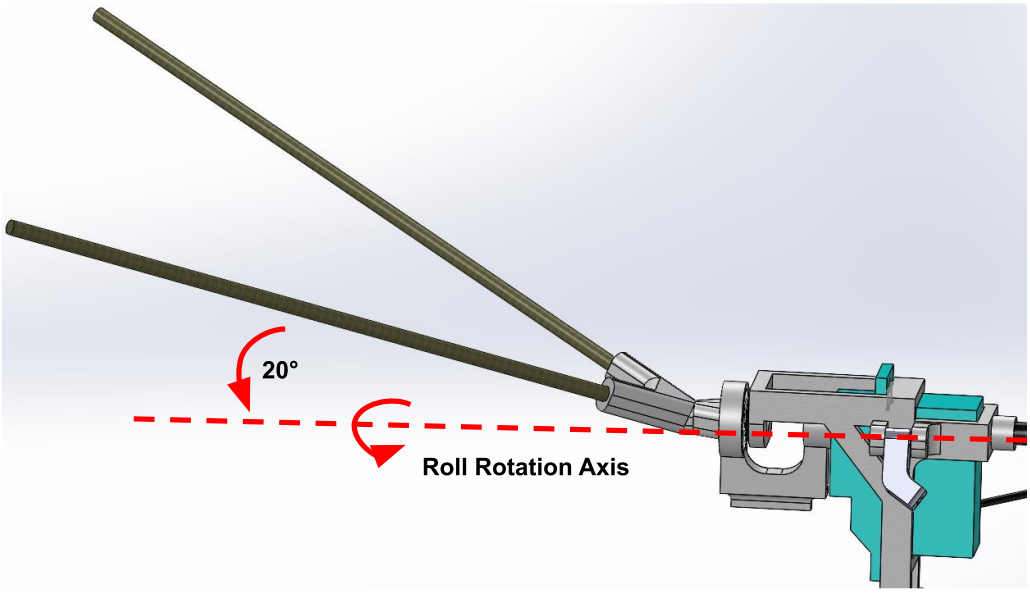

Figure 3.13: Simplified Hind Leg Design

3.8 Additive Manufacturing

Many of the parts from the previous sections have complex geometry. Due to the complex geometry, the need for part consolidation and lightweighting, additive manufacturing was utilized to create many parts. The additive manufacturing process used was FFF (Fused Filament Fabrication). PLA, a layer height of 0.1mm, and a nozzle diameter of 0.04 mm were chosen for a high-resolution print for all but two parts. The print time for all parts but two is 23 hours and 23 minutes, as depicted in Figure 4.13, given a print speed of 50mm/s. Additive manufacturing printers have advanced rapidly, and newer commercial printers that have print speeds of up to 500mm/s have become available, which could significantly reduce the total print time [32].

Additive manufacturing has allowed for highly customized pieces and fast iteration of many parts of VALKRIE, and relatively inexpensive compared to traditional manufacturing, making VALKRIE accessible to any research institute interested in creating one.

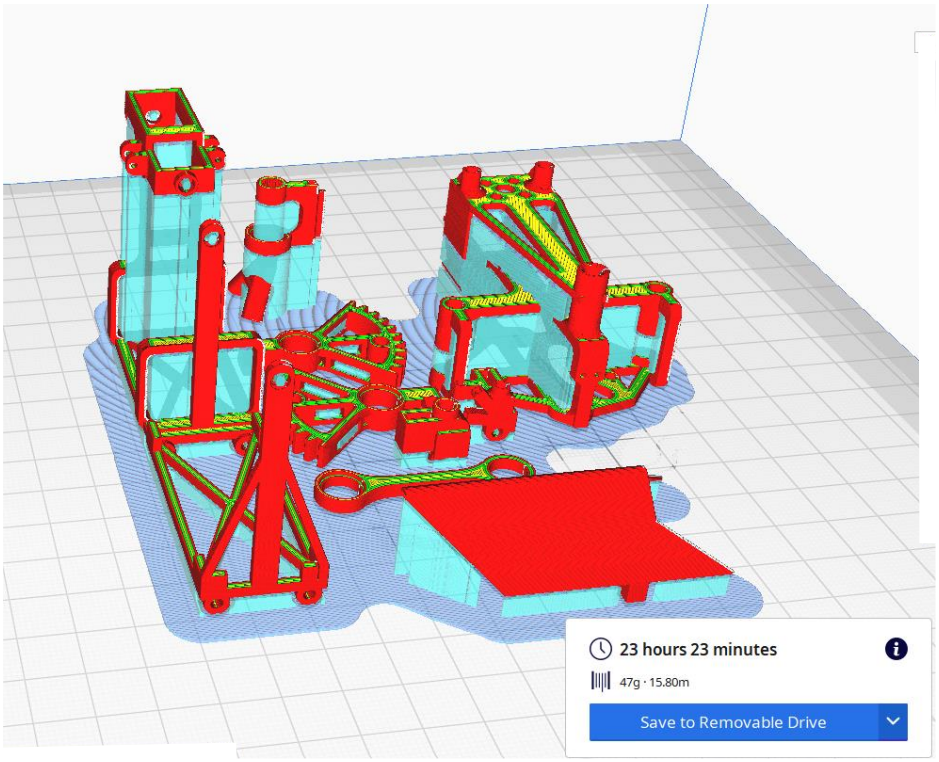

Figure 3.14: Additive Manufacturing Print Preview

The flexible material that acts as a spring for the wing retraction was also created with additive manufacturing to create a custom amount of tension in the wing retraction mechanism. This print was separated from the previous print because of the different materials used. To print these parts, it took a total of 11 min, as shown in Figure 3.15. Additive manufacturing allowed for the easy iteration and customization of the tension to extend the wings.

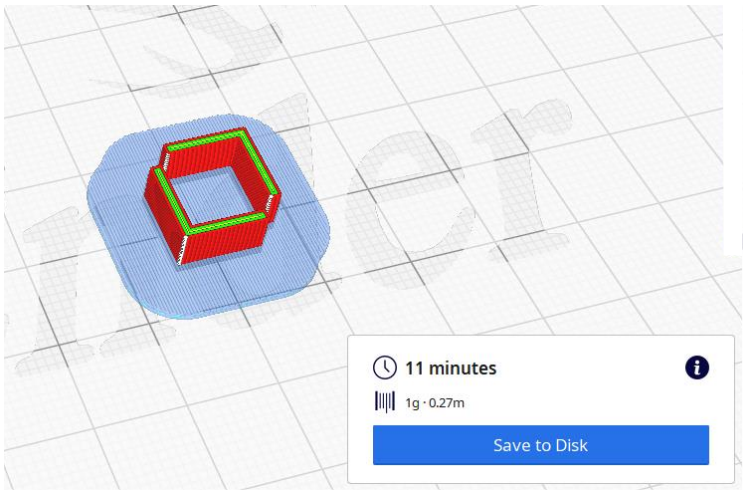

Figure 3.15: Wing Retraction Flexible Material Print

3.9 Weight Distribution

Once all of the components are printed and assembled, the weight of VALKRIE is 82.0 grams. This is considerably lower than other robotic bats that fly: 289 grams and 580 grams, Beihang University and Festo Flying Fox respectively [11][10]. 82.0 grams is, however, more than the weight of *Hipposideros diadema*, which is 46.9 grams. Decreasing the mass while retaining a life-size model to match the biological counterpart proved difficult. Due to the necessary weight of electronics, the frame, wings, and membrane, the weight could not be reduced to 46.9g. A breakdown of the weight by grouped components is shown in Figure 3.16. The initial weight of the first iteration of VALKRIE was 115g. Through various mechanical and electrical design changes, the weight was reduced significantly. Decreasing the total weight of the robot results in increased net lift from the wings. Being such a vital part of the aerodynamics of VALKRIE and to more accurately mimic the biological counterpart, the weight of VALKRIE decreases as much as possible while maintaining functionality.

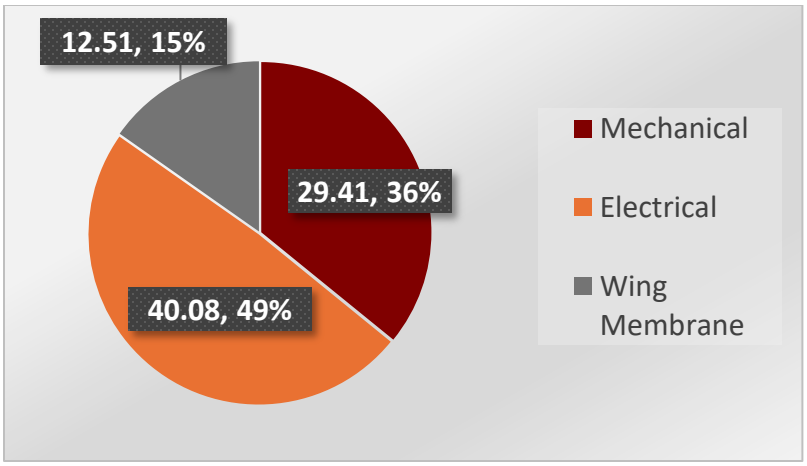

Figure 3.16: Weight Percentage Chart

3.9.1 Mechanical Weight

When designing the mechanical components, the weight was a defining parameter. The weight distribution for the different subcomponents of the mechanical system is illustrated in Figure 3.17; all units are in grams. The mechanical components comprise 34%, or 28.1 grams, of the total weight.

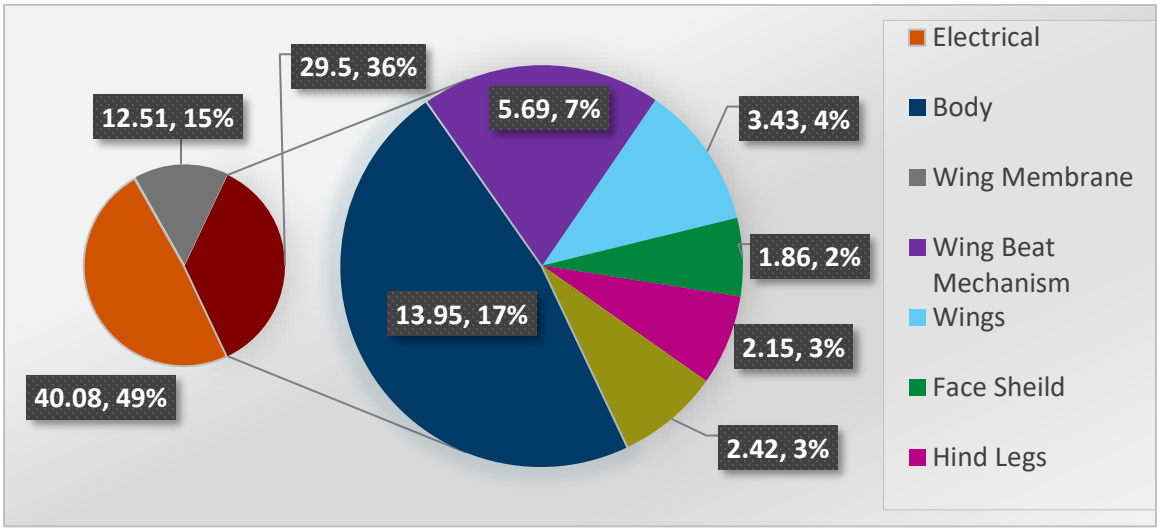

Figure 3.17: Mechanical Weight Distribution Chart

3.9.2 Wing Weight

The ripstop nylon and the natural rubber membranes have different weights. Ripstop nylon material is used more in terms of area, but it has a lower density than natural rubber material. As illustrated in Figure 3.18, the nylon material takes up 6.0% of the total weight, while the natural rubber takes up 9.0%.

With the wing material taking 15% of the total weight, the center of mass shifts up and down during flight. As described in section 2.4, bats maintain a certain wing weight to total weight ratio. Using Equ. (2.2) and the total weight of VALKRIE, the desired weight of the wings would be 14.0 grams. The weight of the wing structure and the wing membrane, excluding the weight of the tail membrane, has a total weight of 15.1 grams. The novel design of the passive wing retraction allows the wings to experience similar inertial power loss while still mimicking the wing retraction of a bat.

Most of the wing's weight comes from the wing membrane. Commercial products were used to create the membrane, limiting the thickness and material available. Other robotic bat projects have synthesized the wing membrane to create a customized thickness and material [4]. To improve upon VALKRIE and lower the weight, the elastic material could be significantly improved by creating a lighter material that maintains the natural rubber's elastic properties.

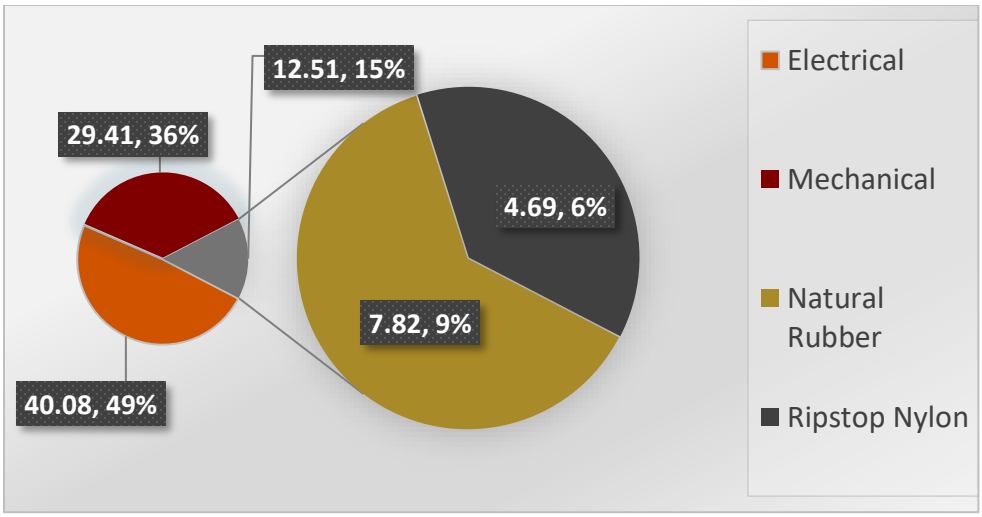

Figure 3.18: Wing Material Weight Comparison

3.9.3 Center of Mass

The weight is significant not only in terms of magnitude but also in location. The center of mass is the point at which all of the matter can be concentrated into a single point at the mean position of the mass. The center of lift is the point at which all lift forces can be represented by a single point at the mean position of all the lift forces. The relationship between the center of lift and the center of mass changes the stability of flight. If the center of mass is too far forward, VALKRIE will nosedive. If the center of mass is too far back, VALKRIE will backflip. Figure 3.19 shows how the center of mass and center of lift affect how VALKRIE's pitch will change. It is desirable to have a center of mass in front of the center of lift because the rotation of the center of lift around the center of mass can be counteracted with the hind legs of VALKRIE.

The center of mass for VALKRIE is 58.5 mm from the wing's leading edge as seen in Figure 3.20. This value accounts for all components including the wing material.

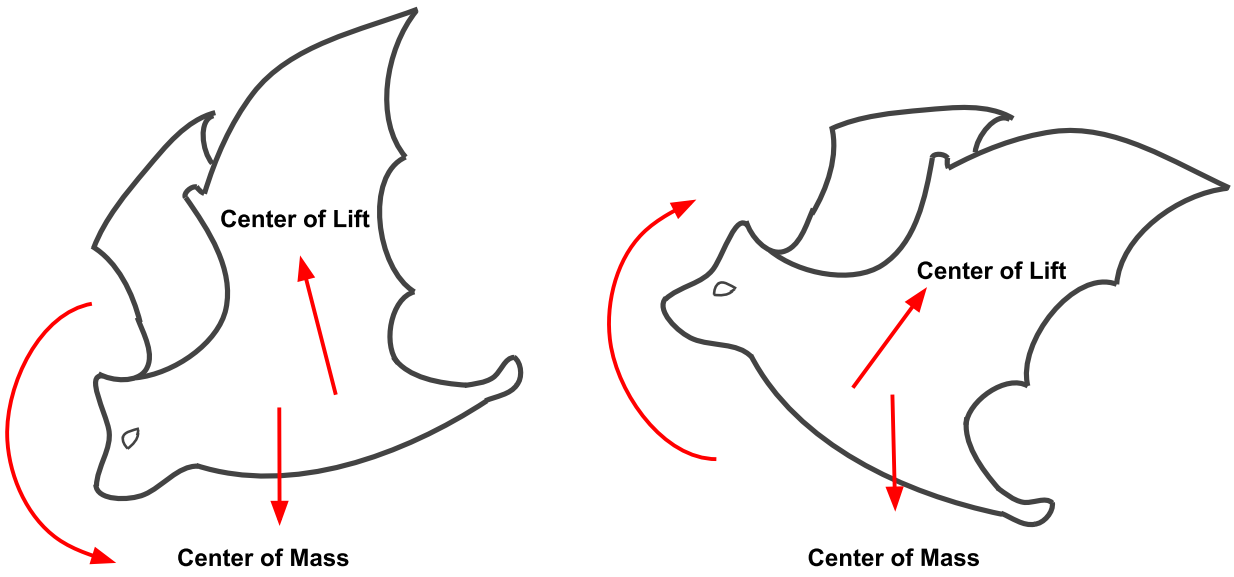

Figure 3.19: Bat Center of Mass and Pitch Affect

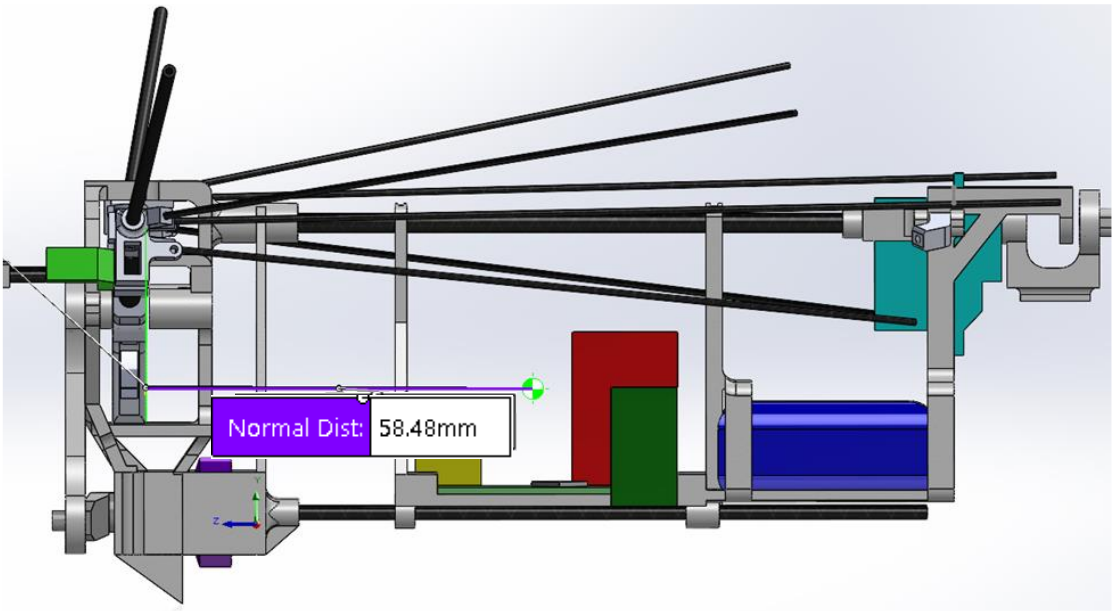

Figure 3.20: Center of Mass CAD

3.10 Change in Pitch During Wing Stroke

The center of mass is not the only factor when stabilizing flight along the lateral axis. The angle of attack for the hind legs counteracts the unbalanced moment caused by the center of mass and center of lift. As shown in Figure 3.21, the hindlegs create a moment opposite to the moment of center of mass around the center of lift.

As VALKRIE rotates forward along the lateral axis, the hind legs have more authority because more surface area interacts with the incoming airflow. The downside to this design is the drag introduced into the system, which decreases the overall flight speed of VALKRIE. The hind legs not only prevent VALKRIE from nose-diving but also steer VALKRIE in a circular motion by turning towards the desired yaw. The integrated roll Proportional Integral Derivative (PID) also controls the hind legs depending on the desired roll received from the operator. While the operator has direct authority over the roll, the roll is coupled with the yaw; so, as the operator and controller change the roll, the desired yaw can be reached.

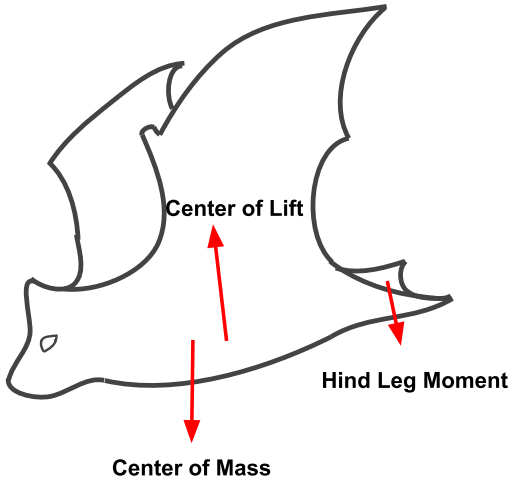

Figure 3.21: Hind Leg Moment Affect

Because the center of mass is not exactly on the center of lift, the pitch goes into a sinusoidal motion for every wing cycle. This sinusoidal motion constantly changes the angle of attack of VALKRIE's wings. Figure 3.22 shows how the angle of attack changes per wingbeat cycle. The change in the angle of attack when the wings flap causes forward thrust and lift [33].

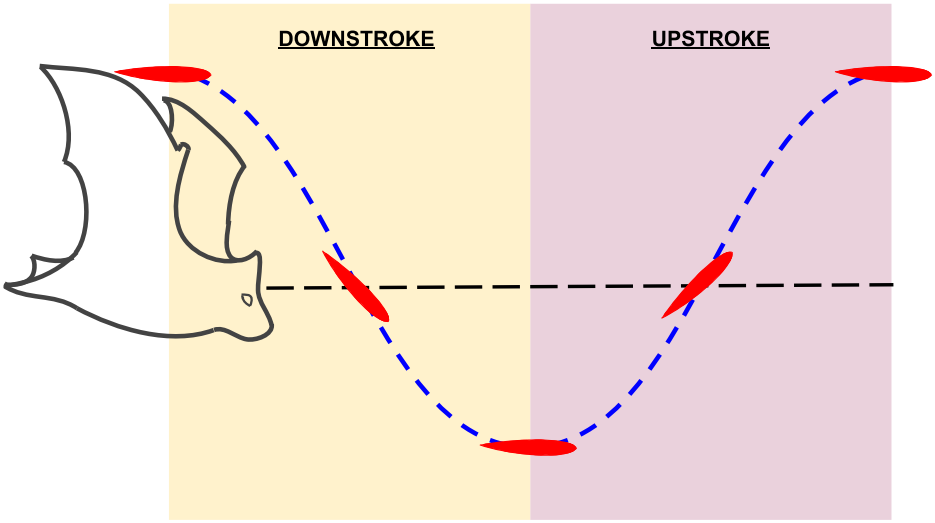

Figure 3.22: Angle of Attack Versus Wing Stroke

Experimental Change in Pitch During Flight Test

Tests were conducted to measure the pitch in order to evaluate if the hind leg moment, center of mass, and center of lift relationship creates a sinusoidal motion on VALKRIE. The tests were also conducted to determine how the time changes between the upstroke and downstroke during flight. As shown in Figure 3.23 (a), the pitch of VALKRIE changes in a sinusoidal motion during flight, similar to the pitch flight pattern of *Hipposideros pratti*. During the test, VALKRIE was given a constant ESC command of 47.4%. The disturbances in the pitch may be due to roll instability that has yet to be corrected or an unaccounted aerodynamic effect. Several tests were conducted to determine the percentage of the time it takes to complete an upstroke and downstroke. The ESC was given a constant command for a consistent output wingbeat frequency to perform these tests. As shown in Figure 3.23 (b), the percent time it takes to generate a downstroke is greater than the percent time to generate an upstroke. This test was measured using a high-speed camera and video software to time the upstroke and downstroke. This experimental data shows that VALKRIE is able to mimic the wing motion of a bat in terms of pitch change and the differing downstroke and upstoke times.

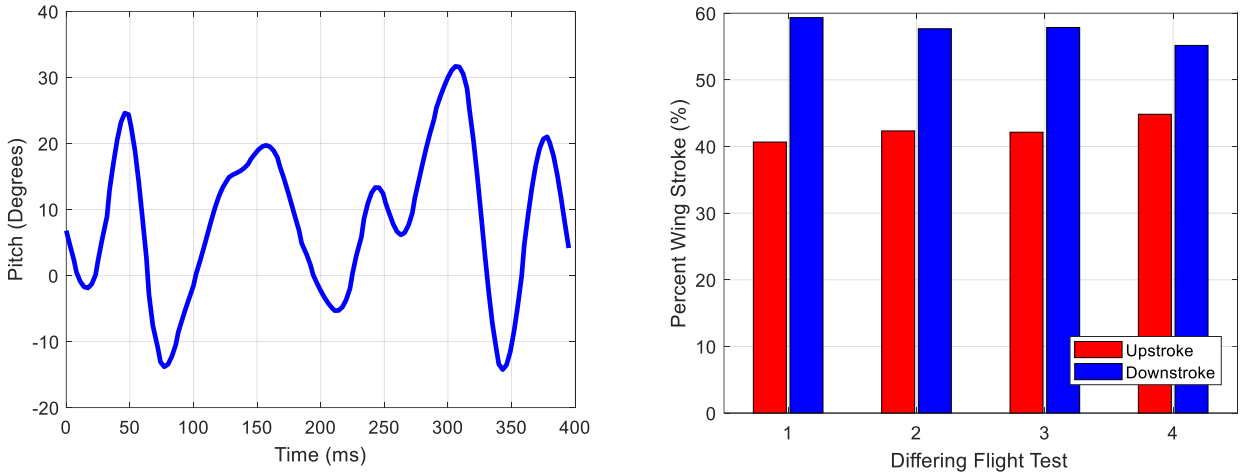

(a) (b)

Figure 3.23: Pitch and Stroke Cycle Experimental Data

3.11 Lateral Stability Design

To have a stable flight in the roll axis, VALKRIE must have a positive average dihedral. A dihedral is the angle of the wing above the center of the body. VALKRIE has an average dihedral of 15 degrees, as shown in Figure 3.24. When the average dihedral is less than 0 degrees, the system experiences lateral instability and is then called an anhedral [34]. The average dihedral assumes that the wing has a fixed area for the duration of a flapping cycle. Since VALKRIE does not have a fixed wing area, the cutoff between stable and unstable is not at an average dihedral of 0 degrees. VALKRIE has less wing area for positive angles because of VALKRIE's wing retraction. Thus, the greater the wing retraction, the more lateral instability VALKRIE will experience.

The flapping amplitude of VALKRIE is 75 degrees: 45 degree dihedral and 30 degree dihedral, as shown in Figure 3.24.

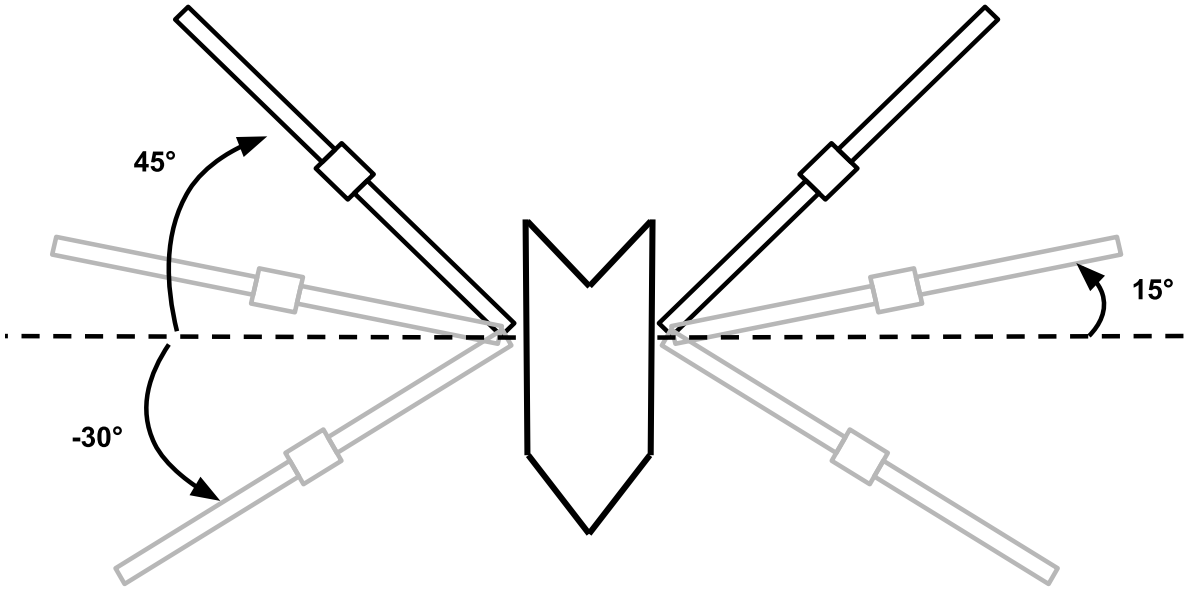

Figure 3.24: Wing Dihedral and Amplitude

3.12 Planform Wing Area and Dimensions

Bats retract their wings during upstroke and extend the wing during downstroke; this wing retraction causes a reduction in the area of the wing [35]. Bats do this because less planform area of the wing during the upstroke means less negative lift produced by the upstroke; this causes a net increase in lift. A study found that the inner wing retraction of *Leptonycteris yerbabuenae* is around a 50% reduction in the area between the maximum and minimum inner wing areas during flight [36]. *Leptonycteris yerbabuenae* has a similar aspect ratio to *Hipposideros diadema*; 7.1 compared to 7.4, respectively [36][3]. To determine the planform wing area of VALKRIE based on the wing's amplitude, a simplified wing model was broken into several different areas, as shown in Figure 3.25. Where L1 is the distance from the center of the body to the wing retraction joint, L2 is the first finger, L3 is the second finger, L4 is the third finger, L5 is the distance between the forearm and the hind legs, and L6 is the length of a hind leg.

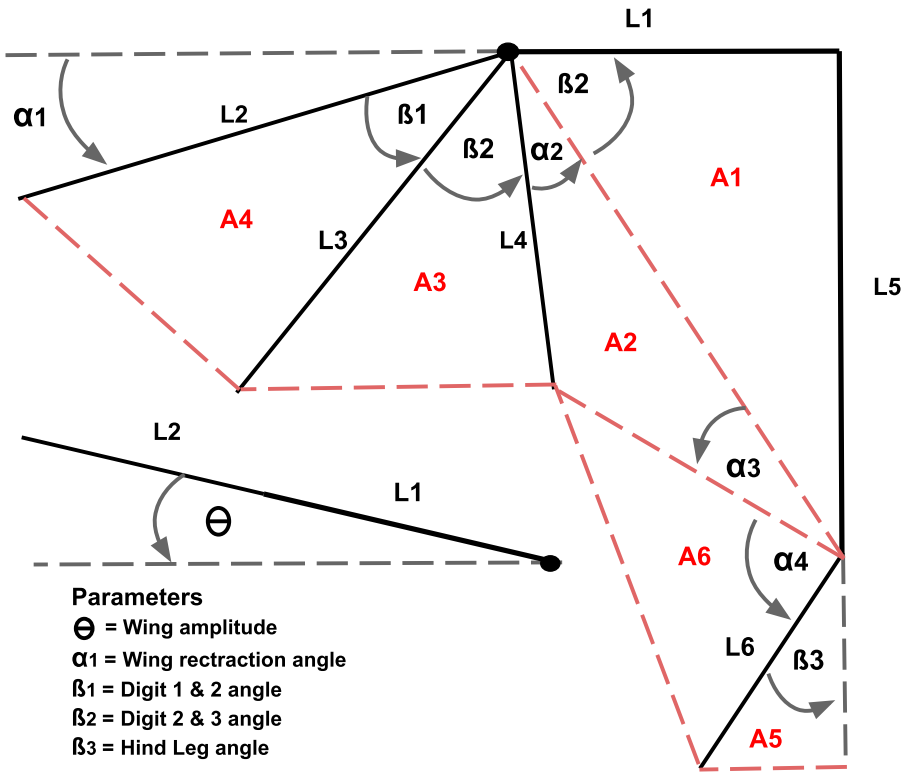

Figure 3.25: Planform Wing Area Dimensions

The total planform wing area was calculated based on the current wing amplitude. From the wing amplitude, the angle at which the hand retracts (α1) can be calculated along with the current planform wing area, where the planform wing area can be computed using Equ. (3.1).

$$A_p\big(\varphi(t),\theta(t),\alpha1(t)\big) = \big(A1(\alpha1) + A2(\alpha1) + A3(\alpha1) + A4(\alpha1) + A6(\alpha1)\big) * \cos(\theta)\cos(\varphi) \qquad (3.1)$$

Where A_p is the planform wing area, θ is the wing amplitude, and φ is the wing's pitch. The wing's pitch was estimated using the average maximum and minimum pitch for the experimental data described in section 3.10, and the phase of *Hipposideros pratti* is shown in Figure 2.6. The frequency of the downstroke compared to the upstroke was calculated using experimental data described in 0. The inputs to calculate the planform wing area are shown in Figure 3.26 (a). The planform area has 45% more area under the curve for the downstroke compared to the upstroke, as shown in Figure 3.26 (b) for a single wing.

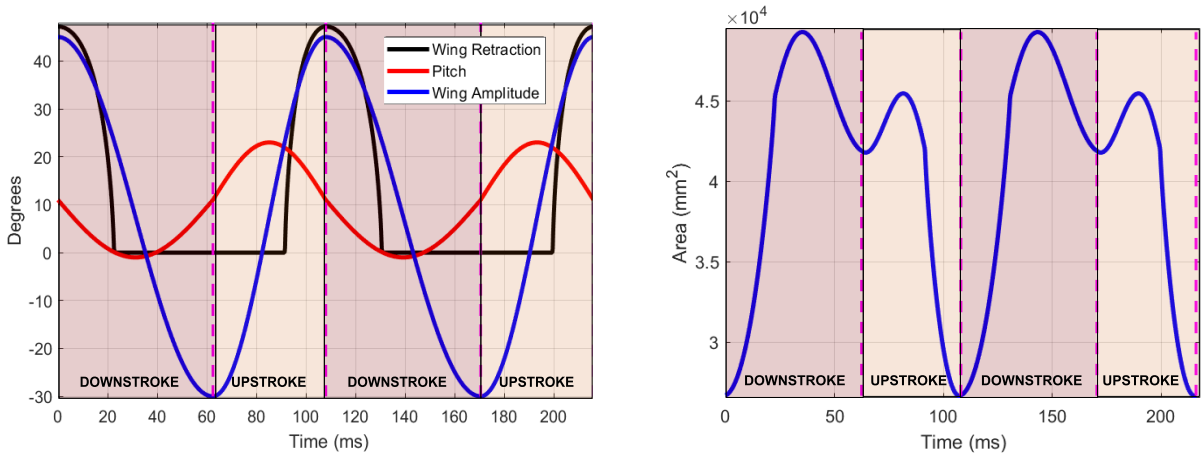

(a) (b)

Figure 3.26: Wing Planform Area Estimation and Planform Inputs

The inner wing area compared to *Leptonycteris yerbabuenae* comprised areas A1, A2, and A6 from Figure 3.25. VALKRIE's estimated maximum planform wing area reduction is 50.0%, matching the wing retraction of *Leptonycteris yerbabuenae*. Figure 3.27 depicts how the wing retracts during the upstroke, decreasing the inner planform area similar to a bat's.

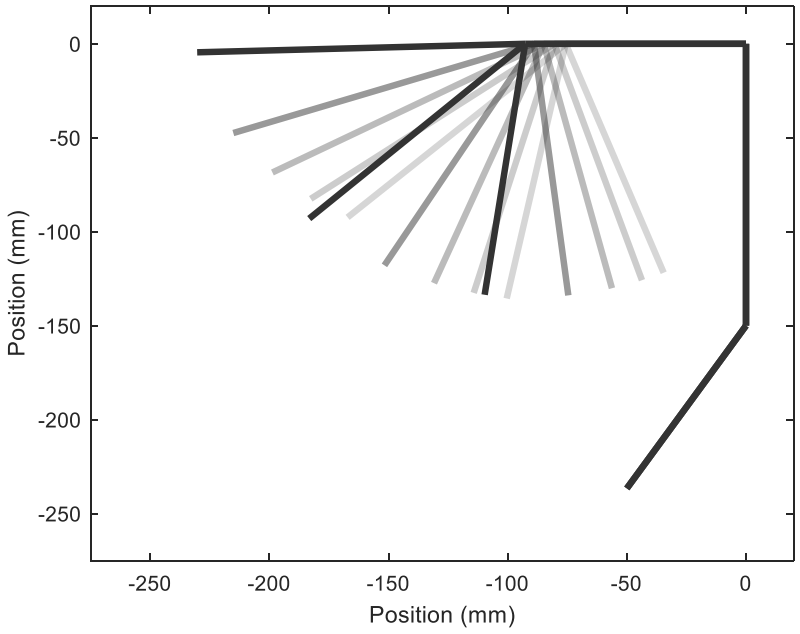

Figure 3.27: Wing Retraction During Upstroke

The passive wing retraction created by the VALKRIE design extends and retracts the same amount during upstroke and downstroke, but the time to retract and extend differs between upstroke and downstroke. Because the downstroke takes more time than the upstroke, this would result in less planform area over time for the upstroke, increasing the net lift. This increase in overall net lift dramatically contributes to the success for the flight of VALKRIE. The other robotic bats of similar size created by other research institutions also have wing retraction, but the complexity of their designs adds weight proportionally larger than that of their biological counterparts. The wing retraction and wing design of VALKRIE can mimic the wing retraction of a bat and maintain the wing weight to the total weight ratio of bats.

The parameters to create a wing retraction of 50% are chosen to match the maximum dimensions of *Hipposideros diadema*'s wingspan and body length. The average lengths of *Hipposideros diadema* were linearly scaled up to match the maximum wingspan, as shown in Table 3.1; all lengths are in millimeters [37] [14]. The L5 parameter for the head-to-body length was not from the same source as the others, so it was not scaled.

Table 3.1: Wing and Body Dimensions

Parameter	***Hipposideros diadema* Mean**	***Hipposideros diadema* Scaled**	**VALKRIE**
L1	85.9	105.6	105.0
L2	127.95	157.4	157.0
L3	118.8	146.1	146.0
L4	113.2	139.2	139.0
L5	190.0	190.0	190.0
L6	68.8	84.6	105.0

While most of the lengths were determined the dimensions of e*Hipposideros diadema*, the hind legs are proportionally larger. The hind legs of VALKRIE are responsible for steering to the right and left and stabilizing the superior from nosediving. The length of the hind legs was increased to compensate for the lack of degrees of freedom and to grant more authority to the hind legs for stabilization and steering.

3.13 Design Accomplishment Overview

VALKRIE successfully mimics and simplifies the complex flying motion of bats through the mechanical design. VALKIRE is able to mimic the wing retraction of bats while maintaining the wing weight to total weight ratio of bats. VALKRIE also retains the size dimensions of *Hipposideros diadema*, with the exception of the hind legs. Through the mechanical design of the hind legs, VALKRIE can create a sinusoidal pitch motion similar to that of a bat in flight. As the mechanical design is responsible for the motion and bio-inspired aspects of a bat, the electrical design is responsible for driving, powering, and controlling the mechanical design.

Chapter 4

Electrical

To drive the mechanical components and control VALKRIE, electronics are vital components of VALKRIE. The downside to having control is the weight contributed by the electronics, and the weight of VALKRIE is one of the most influential aspects when attempting flight. The electronics of VALKRIE comprise 51% of the total weight. The electronic components can be seen in Figure 4.1, including components include the Arduino, battery, brushless motor, ESC, gearbox, receiver, hind servo, voltage regulator, and wires. The weight comparison chart for the electronics is shown in Figure 4.2. The driving factors for choosing the electronic components were meeting minimum functionality requirements and minimizing weight.

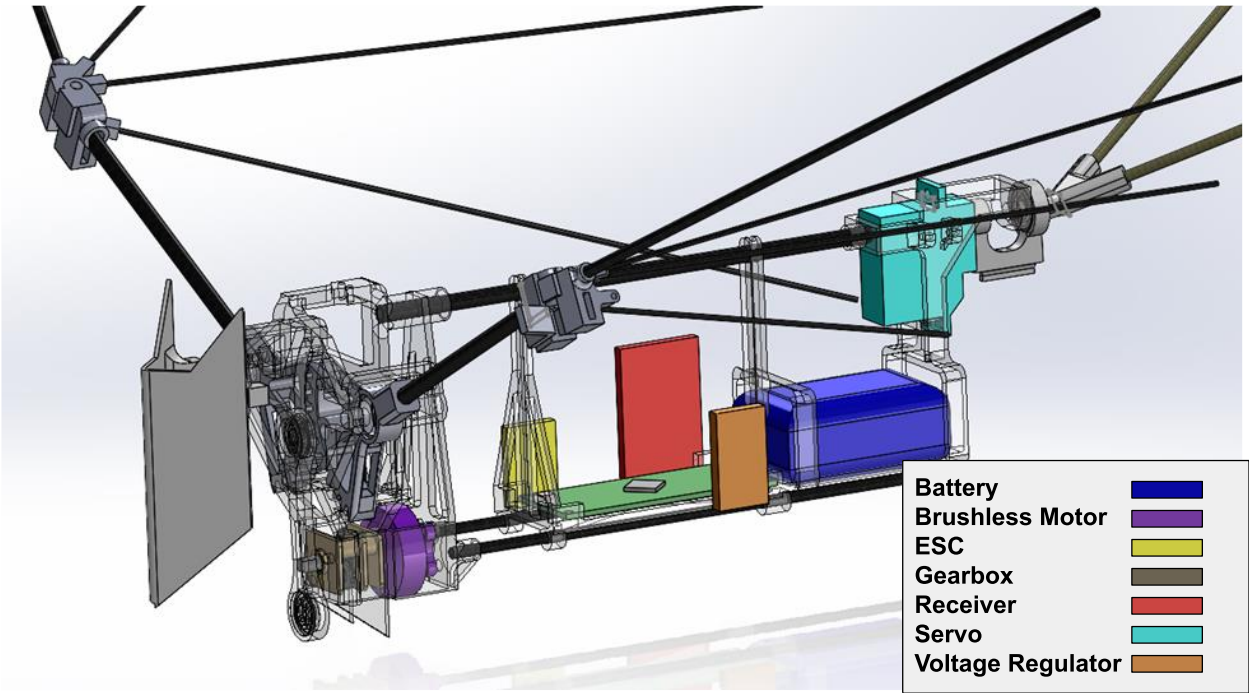

Figure 4.1: CAD Model of Electronic Components

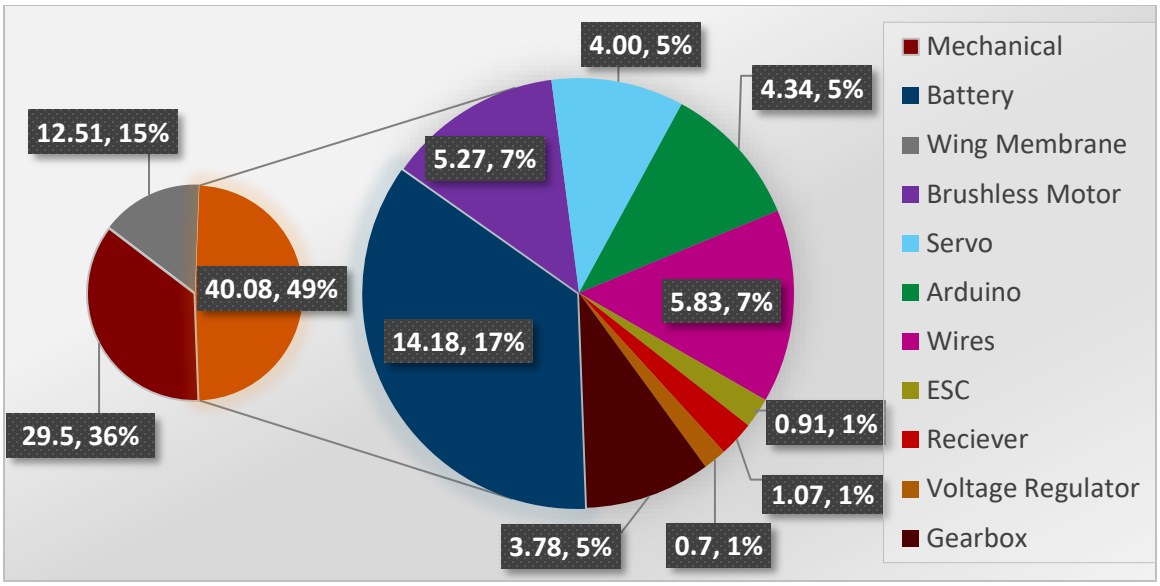

Figure 4.2: Electronic Weight Comparison Chart

4.1 Electrical Communication

The brain of VALKRIE is the microcontroller. The Arduino Nano BLE processes information from the receiver and commands the motors accordingly. The microcontroller has a built-in IMU, the LSM9DS1, as shown in Figure 4.3, that samples the roll and pitch values at 128Hz. The microcontroller calculates the PID for the roll to retain the desired positions. The software is contained within the microcontroller and is denoted in detail in the software section. The main reasons for choosing the Arduino Nano BLE were because it has enough ports for all the inputs and outputs, has a built-in IMU, and weighs only 4.3 grams.

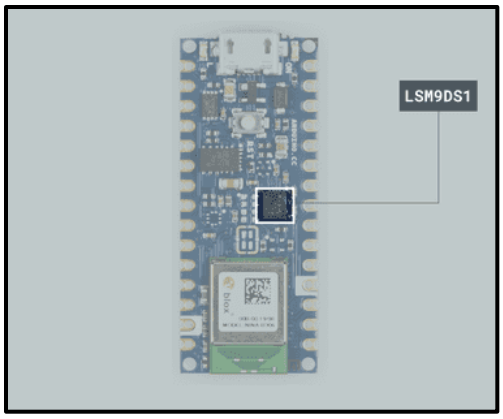

Figure 4.3: Arduino Nano BLE IMU [38]

If the microcontroller is the brain of VALKRIE, the receiver is its ears. A 9-channel Serial Bus (SBus) RF (Radio Frequency) receiver allows communication between the controller and the robot, feeding the roll, pitch, speed, and mode to the microcontroller. The receiver has a range of 600 meters, allowing the operator to control VALKRIE over long distances. The VALKRIE project's initial receiver was the RadioLink R9DS 10-channel receiver. This receiver weighed 8.8 grams. Because not all ten channels were utilized, the VALKRIE currently uses the RadioLink R6DSM, which only weighs 1.1 grams. For serial communication with SBus, the single line must be inverted to be read into the microcontroller.

The AT9S remote controller was chosen to control VALKRIE because it can be highly customized for channel communications. The controller offers a throttle for the speed and a joystick for the pitch and roll commands. The controller also has a three-mode switch to send the current mode to VALKRIE.

4.2 Power Supply

The battery of VALKRIE is the heaviest single component of VALKRIE, weighing 14.15 grams. The 7.4 volt Lithium Polymer (LiPo) battery is a 2-cell battery with 300 milliamp hours. The rechargeable battery provides enough power to last an estimated maximum of 5 minutes and 48 seconds; this measurement was determined by timing sequencual flight test until the wing were unable to flap. A single cell 3.7 volt, 5.9 grams, 220 milliamp hour LiPo

battery was also considered but did not supply enough battery life for longer flights. The 3.7-volt battery would also need a step-up voltage regulator to power the motor sufficiently.

While the battery provides direct voltage to the ESC, a 5-volt step-down voltage regulator is used to stream a steady 5-volt supply line of power to the Arduino, receiver, and servo motor. The hind legs of VALKRIE are controlled by a single servo motor that runs on 5 volts and has a torque value of 0.7 kg-cm. The desired position of the servo is dictated by the microcontroller, allowing for controllability of the hind legs, which enables the operator to turn the robot to the right and left.

4.3 Wing Motor

The driving motor for VALKRIE that creates the flapping motion is a brushless DC motor. Brushless DC motors are standard for UAVs because of their efficiency and speed. The shaft for the motor is attached to a small metal gear using JB Weld, as shown in Figure 4.4; this generates the speed and torque for the flapping motion.

Figure 4.4: Wing Driving Motor with Attached Gear

The calculations for the no-load speed in Hertz after the gearbox are shown in Equ. (4.1), the equation does not account for the efficiency of the gearbox.

$$No\ Load\ Speed = \frac{V * Kv}{N * 60} \qquad (4.1)$$

Where V is the battery voltage, Kv is the RPM per Volt value of the motor, and N is the gear reduction. VALKRIE has a 5000Kv motor and a gear reduction of 50:1; this gives VALKRIE a no-load speed of 12.3Hz. Other Kv motors and gear ratio combinations were also considered and are shown in Table 4.1. The desired Kv values were calculated based on

requiring a loaded speed of 8Hz. All of the following combinations of motor and gearboxes would meet requirements given that the load is under 33% loading and the output speed of the gearbox is 8Hz.

Table 4.1: Available Kv Motor and Gearbox Combinations

Available Gearboxes	Kv Value Required Assuming 33% Loading	Correlated Market Kv motor
5:1	491	500
10:1	983	1000
15:1	1474	1500
30:1	2948	3000
50:1	4914	5000
75:1	7370	7500
100:1	9827	10000
150:1	14741	15000
210:1	20637	21000

The maximum wingbeat frequency during flight is 9.9 Hz; this indicates the motor is running at a maximum of 20% of the stall torque for one wingbeat cycle. This means that the motor is not likely to overheat when operating at maximum speed. The desired wingbeat frequency to match *Hipposideros diadema* is 8.05Hz. VALKRIE can match the estimated wingbeat frequency of *Hipposideros diadema* described in section 2.2 and exceeds the estimated wingbeat frequency by 23%. Because VALKRIE can exceed the estimated required wingbeat frequency, VALKRIE can compensate for the increased mass compared to its biological counterpart, *Hipposideros diadema*, by generating more lift with the higher wingbeat frequency.

Inputs from the operator and microcontroller are not directly wired to the motor. An ESC (Electronic Speed Control) receives inputs from the microcontroller and provides the appropriate voltage to the 3-phase motor. This ESC communicates through Pulse Width Modulation (PWM), so it is controllable by the microcontroller.

Other driving motors were also considered for VALKRIE. A brushed DC motor was used for many iterations of VALKRIE. The 6-volt high-power carbon brush motor came attached to a 50:1 gearbox. This motor has a no-load speed of 650 RPM or 10.83Hz and a stall torque of 0.74 kg·cm. This motor could flap the wings in flight but could not maintain a flapping frequency of 8Hz without being overvoltaged to 7.4 volts. When the motor was overvoltaged to 7.4 volts, VALKRIE achieved enough lift for flight, but the motor would eventually overheat and discontinue to function. However, the gearbox from this motor was used in the current design for VALKRIE because it is a compact metal design, weighing only 3.6 grams. Early versions of VALKRIE used additive-manufactured printed gears to create a custom gear ratio, but they weighed more than 3.6 grams, and with enough use, the gear teeth would wear down. Thus, the metal gearbox that came with the brushed DC motor was used in the final iteration of VALKRIE but not the motor itself.

Another consideration for the driving motor was the servo design. The servo would alternate between two angles, causing the wings to move up and down. This tested design utilized the same model servo used in the hind legs. Several difficulties arose from this design. Firstly, the servo was not fast enough to create an 8Hz flapping frequency. Secondly, when coding, delays would have to be implemented for the desired flapping frequency, increasing the time it takes to run the main loop of the code; this would cause delays in communication and effectiveness of the implemented roll PID and sampling rate. Overall, this design was not chosen, and the brushless motor configuration was chosen.

4.4 Wiring Diagram

All the electrical components and wiring diagrams are shown in Figure 4.5. The red line is the 7.4-volt line. The orange line is the 5-volt line. The black line is ground. The green line is the SBus output from the receiver. The purple line is the output to the ESC. The pink line is

the inverted SBus line. The gray line is the servo line. The brown line is the brushless motor to ESC power lines. Lastly, the maroon line is the 3.3V line.

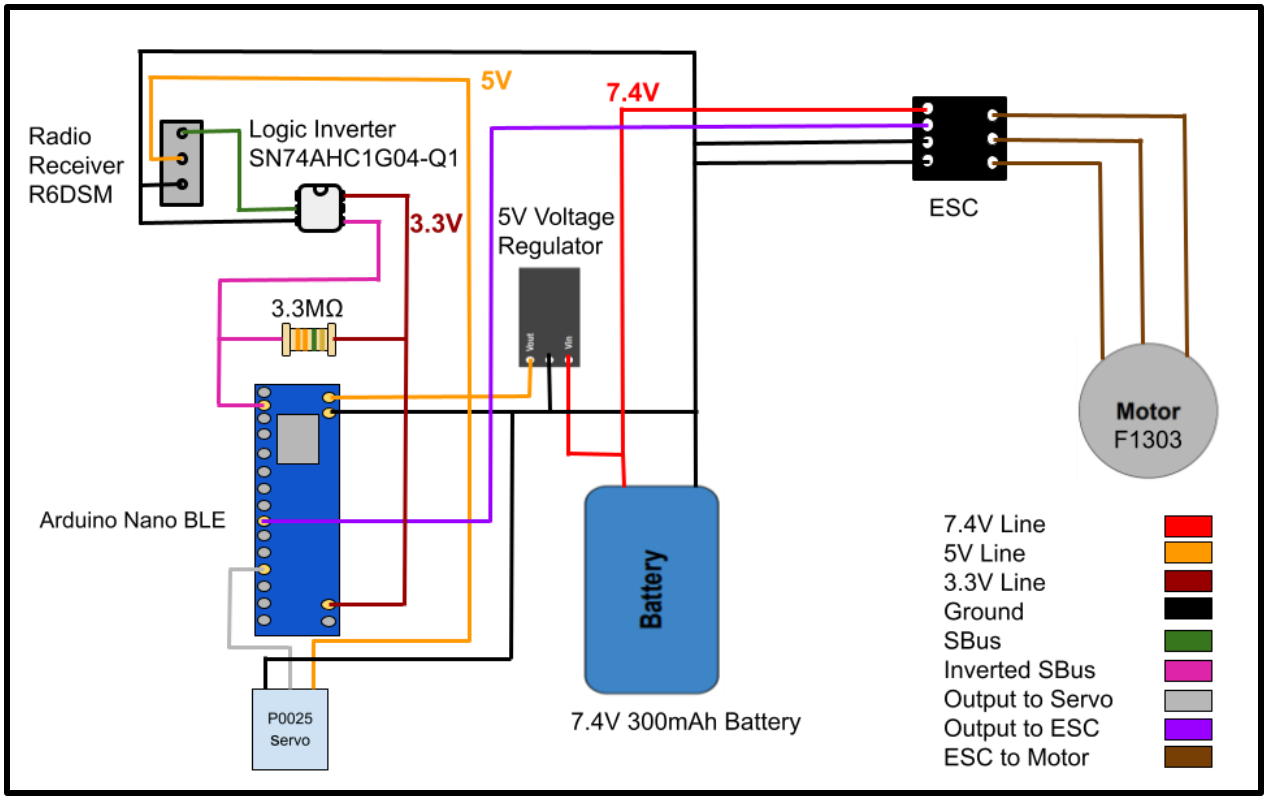

Figure 4.5: Wiring Diagram

Chapter 5

Software

With the hardware chosen, the software and controls can be implemented. Because the Arduino Nano BLE was chosen for the microcontroller, the C++ language was selected for the programming language of VALKRIE. The programming for VALKRIE handles all of the inputs from the receiver, including pitch, roll, and throttle, and then calculates all necessary outputs and saves all desired values. Once the calculations are complete, the software sends the outputs to the ESC and servo motor. A flowchart for the software is shown in Figure 5.1.

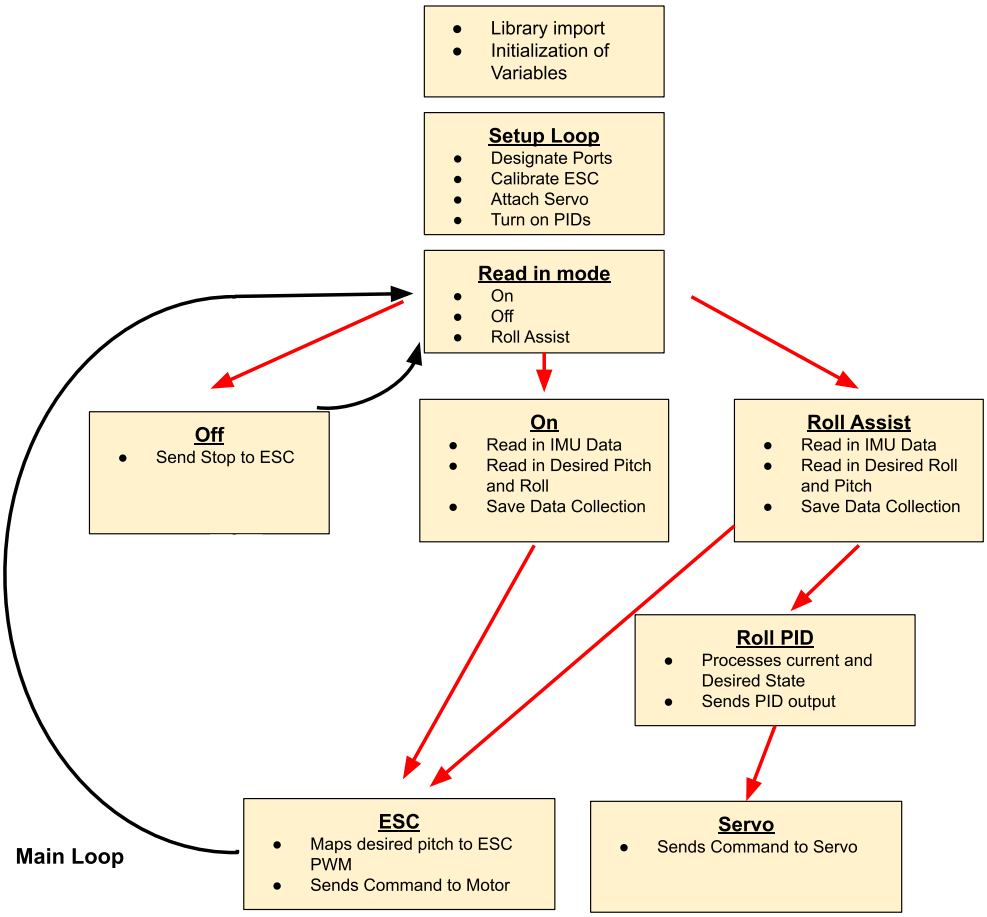

Figure 5.1: Software Flow Chart

5.1 Code Initialization and Setup

Before the microcontroller can send any outputs, the controller initializes four libraries: *Arduino_LSM9DS1.h*, *PID_v1.h*, *ReefwingSBUS*.h, and *Servo.h*. The LSM9DS1 library is the library for the built-in IMU of VALKRIE. This library initializes the IMU to sample at 952Hz and has an acceleration range of -16g to 16g. The library also provides functions that output angle values for the roll and pitch of the Arduino. The PID library has functions that take in a current value, desired value, proportional gain, integral gain, and derivative gain and calculate the output value. The SBus library allows for communication from the receiver through SBus. The servo library allows communication with the hindleg servo but is also used to communicate with the ESC.

All input and output ports are designated in the setup loop, and the servo outputs are designated for the servo and the ESC. After the ESC is set as a servo, it is calibrated by sending the 'STOP' PWM signal. The roll PID is also turned on during the setup loop.

5.2 Main Loop

With everything initialized, the main loop can read the data, process the data, calculate the outputs, and send the appropriate outputs to the hind leg servo and the driving motor. The max time it takes to run through the main loop once is an average of 2.937 milliseconds or 340Hz. This frequency is the sampling frequency, as the main loop collects one set of data every time the loop is run.

5.2.1 Input Data

The microcontroller reads in current roll and pitch values from the IMU and reads in desired roll, pitch, and mode from the receiver through SBus communication.

The input data from the operator and the IMU data set the current and desired values for the current state. The current value is estimated by averaging the data over the previous wingbeat. The wingbeat period is estimated by taking the previous ESC output and mapping it to a wingbeat frequency. Other ornithopters have used averaging the pitch for data [39].

With the current and desired values known, they are run through a PID controller to correct for roll error—a mapping of the current and desired values is shown in Figure 5.2.

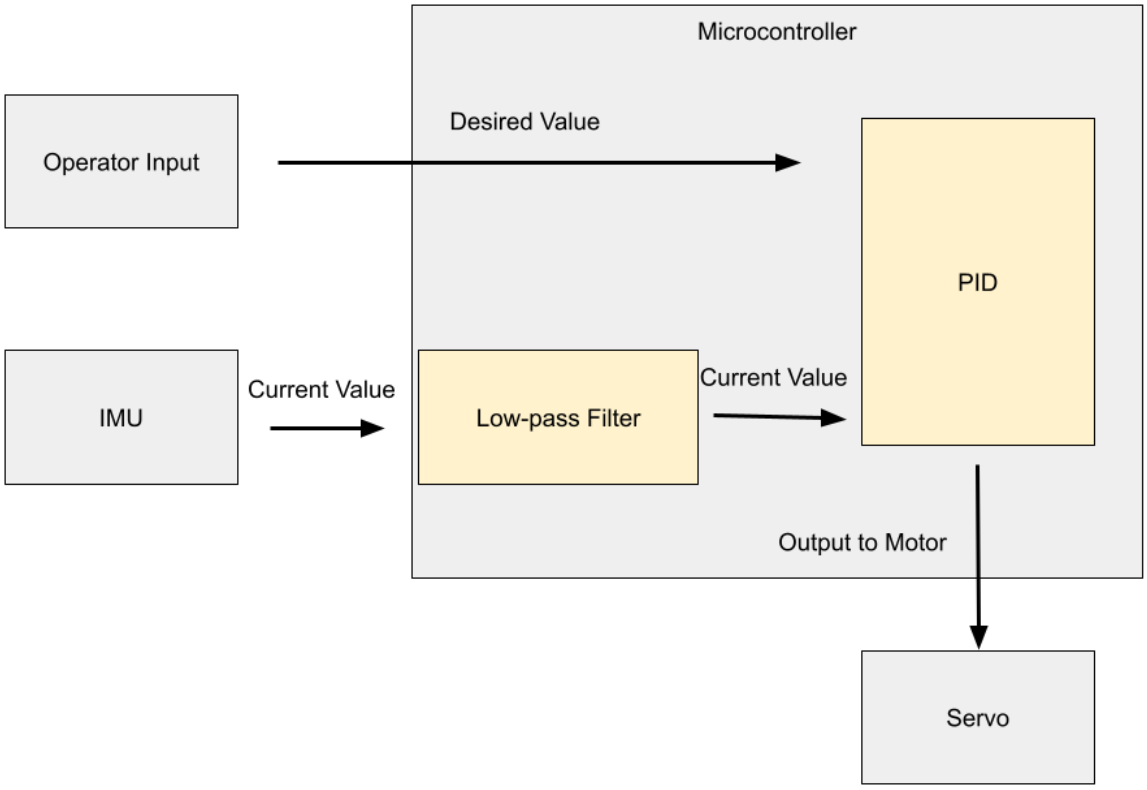

Figure 5.2: Roll PID Current and Desired Values Mapping

5.2.2 Estimating Pitch

Because the pitch changes as a sinusoidal motion because of the aerodynamics, the current pitch value for a single loop does not accurately represent the average pitch per wing cycle. The pitch data is run through a lowpass filter with a cutoff frequency of 10Hz. To compensate for the change in pitch, the data is exponentially smoothed with Equ (5.1).

$$s_t = \alpha x_t + (1 - \alpha) s_{t-1} \qquad (5.1)$$

Where s_t is the smoothed data, and alpha is the smoothing factor. The raw, filtered, and smoothed pitch data is shown in Figure 5.3. The smoothing factor for VALKRE is 0.008.

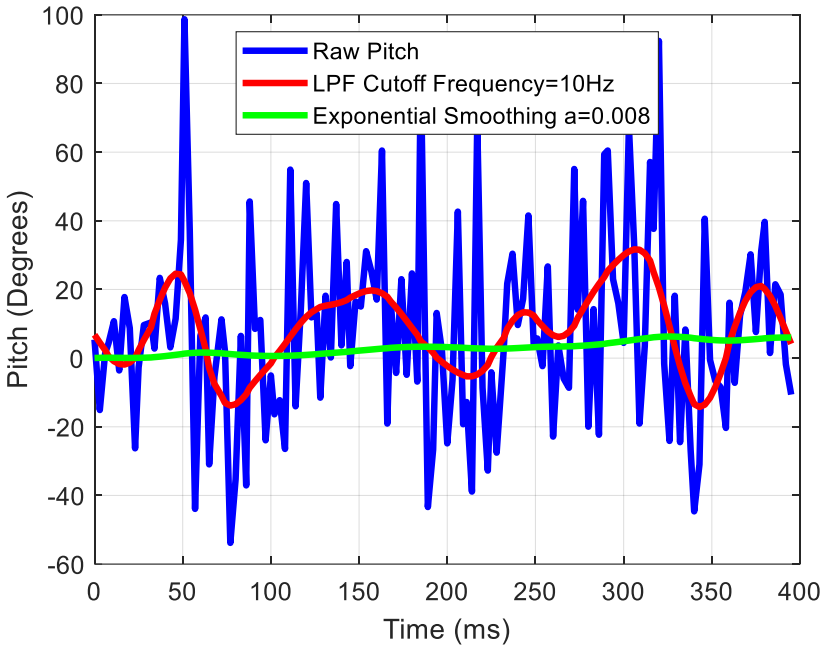

Figure 5.3: Raw, filtered, and smoothed pitch data with constant ESC output of 47.5%

During the test for Figure 5.4 (a), VALKRIE flew at a relatively stable altitude. This value estimates the output to ESC to produce a relatively stable flight. Figure 5.4 (b) shows the pitch for when the ESC is given the ESC command to gain altitude. As expected, the ESC command to gain altitude is less than the ESC command to maintain altitude, 42.6% and 47.4%, respectively. The graphs show that the higher output command produces an average lower pitch; with 42.6% and 47.4% inputs, the respective average pitches are 3.85 degrees and 2.33 degrees. This is because higher frequencies cause more lift, and when the center of lift is behind the center of mass, this will create a larger moment around the center of mass and a resulting decrease in pitch.

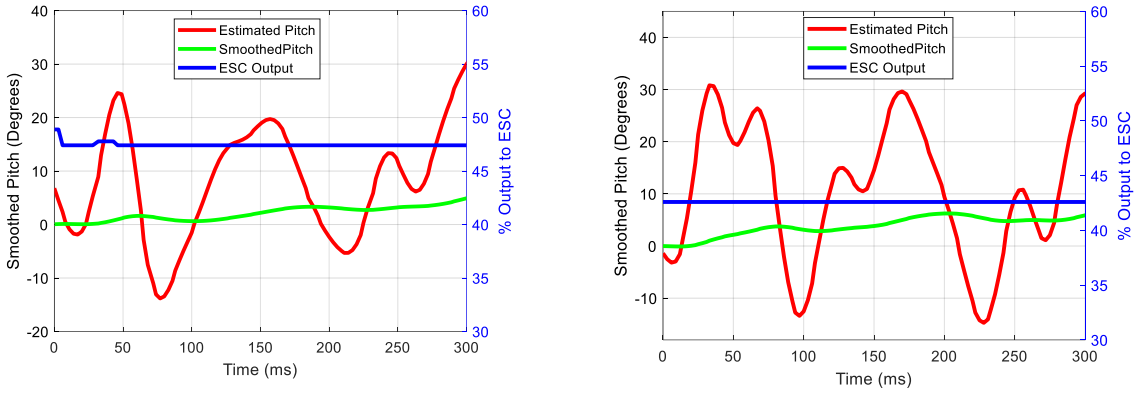

Figure 5.4: Output Command to ESC Effect on Pitch

5.2.3 Modes

Three modes are programmed into the Arduino: off, manual, and roll assist. The off mode sends the stop PWM to the motor. The manual mode allows the operator complete control over wingbeat frequency, pitch, and roll. The roll assist mode does have a PID to automate the roll to maintain a steady lateral stability. A three-way switch and the remote controller operator determine these modes. Switching out of 'off' starts the data collection.

5.2.4 Controlling Roll

To mitigate the disturbances induced by the system, the roll is passed through a low pass filter with a cutoff frequency of 10Hz. When VALKRIE has an error in roll, the hindlegs rotate in the opposite direction to correct the roll. The desired roll was set to 0 degrees to test the roll for stable flight. As shown in Figure 6.7, the hindlegs correct the error and bring the error to the desired value.

The PID controller can correct the roll to maintain a stable flight. The final gains for the roll PID controller are a K_p of 1.6, a K_I of 0.2, and a K_d of 0.04. These gains were iterated with test flights with a constant output to the ESC. The gains were iterated to decrease the correction time and not to overcorrect and cause overshooting. The roll controller took far less time to iterate than the pitch controller. This is because the roll controller's input and output are in degrees, whereas the pitch controller has an input in degrees and an output that correlates to the wingbeat frequency, which was far more complex to iterate.

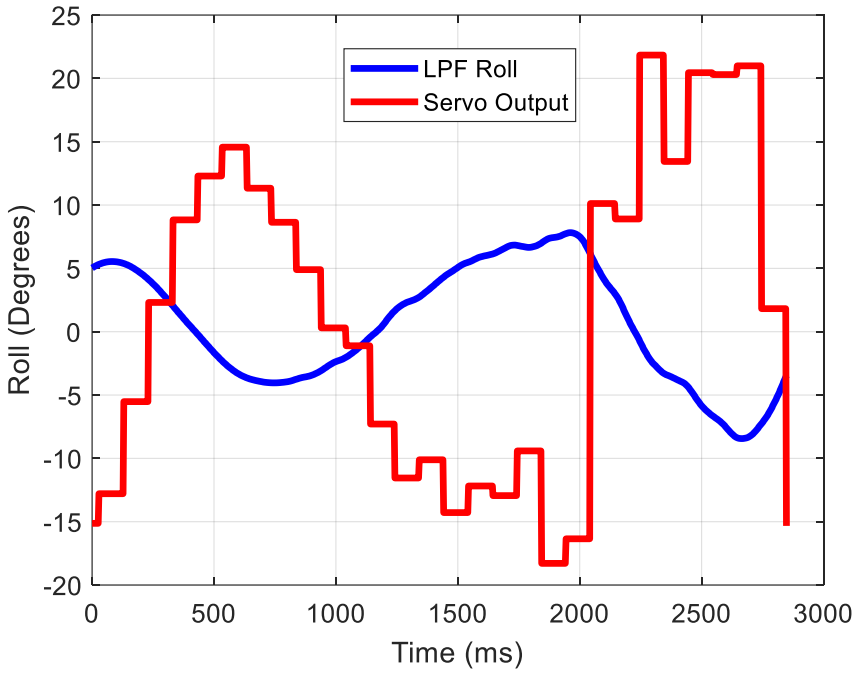

Figure 5.5: Roll PID Control

5.2.5 Saving Data

For analyzing the results, the data for the pitch, estimated pitch, roll, output to ESC, output to servo, and the time stamp are all saved locally at the end of the main loop. When commanded through serial communication with a computer, a flag is set, and the microcontroller will output all of the saved data through the serial port. The data can then be parsed and analyzed.

Chapter 6

Assembly and Build Cost

With all of the parts manufactured and ordered, VALKRIE can be assembled. This section presents the tools and expertise required to build VALKRIE. The costs of VALKRIE can be also broken down for all of the components.

6.1 Assembly

Once all the parts are printed for VALKRIE, the entire assembly can take less than a day. Assembly time varies greatly depending on soldering and tooling ability. The construction of VALKRIE does not require any specialized tooling, requiring only a caliper, pliers, a rotary tool, scissors, an Allen wrench, a soldering kit, a vise, super glue, and double-sided tape.

The electronics were soldering according to the wiring diagram described in section 4.4. A PCB (Printed Circuit Board) was used for soldering the connections together, as shown in Figure 6.1.

Figure 6.1: PCB Wiring

The carbon fiber rods were all cut with a rotary tool with a cut-off-wheel attachment. A caliper with an accuracy of 0.01 mm was used to measure the lengths of the carbon fiber rods. The carbon fiber rods were slid into the respective holes and adhesively kept in place with ordinary Loctite superglue. The ball bearings are pressed in using pliers and are also adhesively held in place with ordinary Loctite super glue.

The membranes are cut using scissors and are attached using double-sided tape and standard Loctite super glue.

Rubber bands keep the microcontroller in place and prevent it from moving in the pitch direction. The rubber bands can keep the microcontroller attached to the chassis in flight but also allow it to be removed for serial connection.

The most challenging process for the assembly is attaching the gear to the motor shaft. First, the gearbox must be removed from the brushed motor it comes attached to by removing the two screws on the front of the gearbox. The gear is removed from the shaft using a rotary tool with a cut-off wheel attachment. The motor shaft is then reduced to a diameter of 0.99 mm. To reduce the shaft, the motor was mounted in a vise, turned on, and then the shaft was iteratively shaved down with a rotary tool and cut-off wheel attachment and measured with a caliper. The gear is then adhesively attached to the shaft with green Loctite.

6.2 Cost Breakdown

The total cost of VALKRIE is relatively low with a total build cost of $240.05 for just one build and a cost of $129.68 per build if building multiple. A complete breakdown of the cost is shown in Table 6.1. This cost analysis does not include any cost for tooling, but VALKRIE does not require any specialized tooling. The most considerable tooling price would be an FFF printer, which ranges significantly in price.

Table 6.1: Breakdown of Part Cost

Part	Amount Per Build	Price ($)	Price Per Build ($)
PLA (1000g)	47g	18.99	0.89
Ball Bearings (10 pk)	7pc	9.99	6.99
Rubber Bands (1000 pk)	7pc	8.50	0.06
3mm Hollow Carbon Fiber (4000mm)	250mm	10.57	0.66
2mm Hollow Carbon Fiber (2000mm)	660mm	9.99	3.30
1mm Carbon Fiber Rod (4000mm)	854mm	9.49	2.02
TPU (250g)	1.00g	17.99	0.07
Total		**85.52**	**14.00**

Part	Amount Per Build	Price ($)	Price Per Build ($)
Gearbox	1pc	7.9	7.9
Wires (6000mm)	500mm	6.88	0.57
Brushless Motor	1pc	15.9	15.9
Servo (5 pk)	1pc	21.99	4.40
Arduino Nano	1pc	29.99	29.99
ESC	1pc	15.99	15.99
Voltage Regulator	1pc	9.99	9.99
Receiver	1pc	17.99	17.99
Battery	1pc	11.99	11.99
Total		**138.62**	**114.72**

Ripstop Nylon Membrane (2,160 in^2)	96 in^2	8.95	0.40
Natural Rubber Membrane (500 in^2)	40 in^2	6.96	0.56
Total		**15.91**	**0.95**

Grand Total	**240.05**	**129.68**

As shown in Figure 6.2 and highlighted in orange, the electronics make up most of the total cost for VALKRIE, whether considering one or multiple builds, 58% or 79%, respectively. Due to additive manufacturing, the price for the mechanical parts (highlighted in red) is only 36% or 14% of the total cost for building one or multiple builds, respectively. Contributing the least amount to the total cost for a single build, the wing membrane only comprises 7% or 11% of the total build cost for one or multiple builds, respectively.

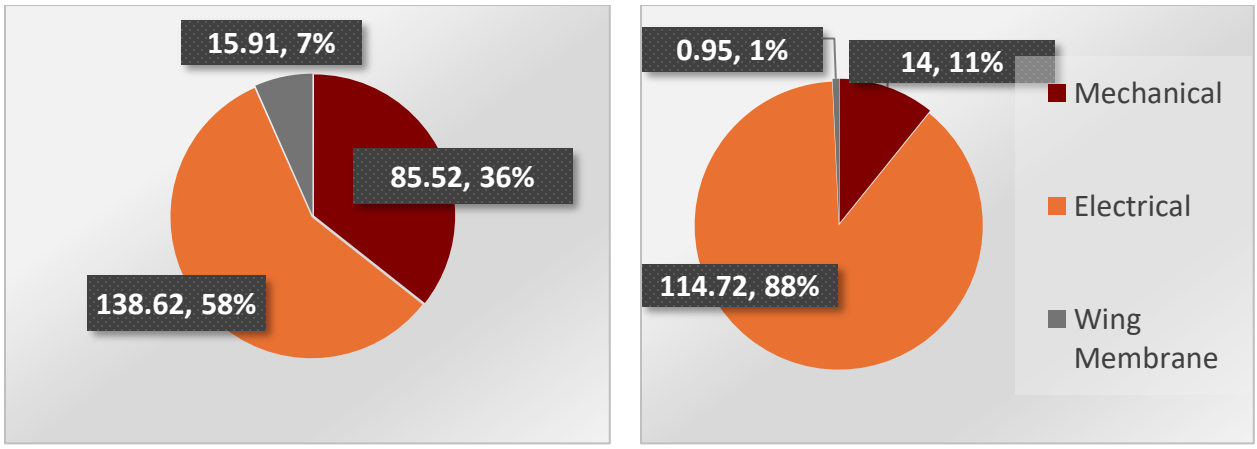

Figure 6.2: Cost Distribution of Multiple and Single Builds

Chapter 7

Testing

Once VALKRIE is fully assembled, VALKRIE can be tested. VALKRIE was tested many times to iterate parameters and gains that eventually led to stable flight. Because VALKRIE has PID's for the pitch and roll, the gains were iterated by testing VALKRIE multiple times in a controlled environment. After the gains were determined, VALKRIE was tested outdoors to determine the flight time and distance.

7.1 Flight Testing

Testing was conducted both indoors and outdoors. Because VALKRIE is susceptible to water, testing was conducted on days without precipitation for outdoor testing. To prevent damage, VALKRIE was also tested on grassy areas. VALKRIE was tested over multiple days with different wind speeds. The wind speed at the time of testing was noted, and VALKRIE was thrown towards the incoming wind to prevent the wind from assisting in flight. The wind index and a compass were used to determine the direction of the wind. VALKRIE was also tested indoors to iterate the PID gains in a controlled environment.

The following steps were taken when testing VALKRIE:

- Turn on the remote controller.
- Power on VALKRIE.
- Wait for the ESC to be calibrated.
- Switch VALKRIE out of off mode.
- Set the throttle to maximum.
- Launch VALKRIE, gripping the chassis at the center of mass.
- Film VALKRIE with slow motion camera.
- Once VALKRIE hits the ground, set throttle to minimum.
- Wait one minute for data collection to complete.

- Connect VALKRIE to the serial port for data collection.

The microcontroller saves the current pitch, smoothed pitch, smoothed roll, output to the ESC, output to the servo, desired pitch and roll, and time. Data collection starts when switched out of off mode and collects 1000 data points (~64.5 seconds) for each variable. The wingbeat frequency is calculated using the high-speed camera; the wingbeat frequency is calculated using Equ. (7.1).

$$f = \frac{Number\ of\ Wing\ Cylces}{Total\ Time} \tag{7.1}$$

Multiple tests for VALKRIE were conducted to find the effects of wind and the maximum wingbeat frequency, as shown in Table 7.1. The wind data was based on the maximum gust wind index for the exact time of the test according to a weather app. The flight speed was also calculated indoors using Equ. (7.2), measuring the displacement from the launching point to the landing point with a tape measurer and the flight time using the high-speed camera.

$$V(m/s) = \frac{Displacement\ (m)}{Total\ Time\ (s)} \tag{7.2}$$

The maximum flight speed for VALKRIE is around 8.3 m/s. This is for displacement and does not consider the trajectory's curved distance, meaning the flight speed calculated is a lower-end estimate of the flight speed. A GPS or other global positioning sensor would be needed to calculate the instantaneous velocity during flight accurately.

Table 7.1: Experimental Data for Wingbeat Frequency, Wind, and Flight Speed

Date	Time (sec)	Cycles	Frequency (Hz)	Wind (mph)	Throttle Input (%)	Flight Speed (m/s)
2/7/24	2.21	19	8.6	6	100	3
2/11/24	1.95	18	9.2	Indoors	67	8.1
2/11/24	1.21	12	9.9	Indoors	100	8.3
2/11/24	1.11	11	9.9	Indoors	100	8.2
2/11/24	1.65	16	9.7	Indoors	100	8.3

Through many tests, VALKRIE could gain altitude and sustain flight when the wind was below 4 mph. Because VALKRIE relies on its wing membrane for flight, the wings are susceptible to wind. This creates increased drag when facing the wind and increased thrust when flying in the direction of the wind. Snapshots of an outdoor test are shown in Figure 7.1 where (a) and (c) are examples of the minimum amplitude in flight and Figure 7.1 (b) and (d) are examples of the maximum amplitude.

(a) (b) (c) (d)

Figure 7.1: Outdoor Flight Test Snapshots

A sustained flight for VALKRIE is having the ability to maintain or gain altitude in flight. A glider can stay in the air for an extended period of time but does not obtain true flight. Since VALKRIE is able to stay in the air and increase in altitude, VALKRIE is capable of sustained flight.

7.2 Weight Determination

For weight determinations, a scale with an accuracy of 0.01 grams was used on each piece and for the total weight of VALKRIE, as shown in Table 7.2. Highlighted in red are the mechanical parts, highlighted in orange are the electrical parts, and highlighted in grey are the wing membranes. The total weight of VALKRIE is 82.0 grams.

Table 7.2: Measured Weights of Individual Pieces

Part	Weight (g)	Quantity	Total (g)
Body Chassis	7.38	1	7.38
Shoulder Gear Right	1.24	1	1.24
Shoulder Gear Left	1.39	1	1.39
Ball Bearings	0.39	7	2.73
Driving Wingbeat Cams	0.72	1	0.72
Hind Leg Rod	0.38	2	0.76
Hind Leg Mount	1.00	1	1.00
Electronic Chassis	5.18	1	5.18
Rubber Bands	0.10	3	0.30
Spine Rod	0.61	1	0.61
2mm Chassis Rod	0.24	2	0.48
Face Sheild	1.86	1	1.86
Flexible Material Tensioner	0.21	2	0.42
First Finger Digit	0.60	2	1.20
Second Finger Digit	0.17	2	0.34
Third Finger Digit	0.16	2	0.32
Wing Support Rod	0.31	2	0.62
Wing Arm Rod	0.43	2	0.86
Wing Retraction Connectors	1.00	2	2.00
		Total	**29.41**

Part	Weight (g)	Quantity	Total (g)
Gearbox	3.78	1	3.78
PCB Board	0.52	1	0.52
Wires	5.31	1	5.31
Brushless Motor	5.27	1	5.27
Servo	4.00	1	4.00
Arduino Nano	4.34	1	4.34
ESC	0.91	1	0.91
Voltage Regulator	0.70	1	0.70
Receiver	1.07	1	1.07
Battery	14.18	1	14.18
		Total	**40.08**

Ripstop Nylon Membrane	4.69	1	4.69
Natural Rubber Membrane	7.82	1	7.82
		Total	**12.51**

		Total	**82.0**

7.3 Loading Tests

VALKRIE can maintain a stable flight and gain altitude; because of this, VALKRIE can carry a payload. To create a payload that could give valuable data, a camera was mounted to the face shield of VALKRIE, as shown in Figure 8.1, and the battery was shifted back to mitigate the change in center of mass caused by the camera.

Figure 7.2: Camera Mounted on Face Sheild

This camera added 5.0 grams to the weight of VALKRIE, making the total mass 87.0 grams. This 600TVL camera came attached to a 5.8 GHz transmitter that can send the live video feed to a receiver that can be viewed on a monitor or Virtual Reality (VR) headset.

With the additional payload of the camera, VALKRIE could not sustain flight. Several reasons would cause VALKRIE not to be able to maintain flight. One reason is that VALKRIE cannot generate enough lift to carry the load. Another reason could be that the additional load shifted the center of mass too much and caused too much weight in the front.

While this iteration of VALKRIE could not carry 5.0 grams, there was additional testing with a 4.3 grams payload attached on the bottom of the electronics chassis. VALKRIE was able to increase altitude with a payload of 4.3 grams at the center of mass. The input for this indoor test to the ESC was a constant 67% output to the ESC, which produced a wingbeat frequency of 9.0 Hz, slightly lower than without the additional loading. Since VALKRIE is able to carry an additional payload, further sensors, such as a GPS sensor, altimeter, LIDAR, etc., have the

potential to be placed on VALKRIE. Being able to carry a payload makes VALKRIE more viable to be used for the many applications of mini-UAVs. There is potential for image recognition, autonomous flight, and further maneuverability and complex flight patterns with the use of further sensors.

Chapter 8

Conclusions

Many robots have attempted to mimic the complex flying motion of bats. VALKRIE successfully mimics the wingspan and head and body length of *Hipposideros diadema* while maintaining the ability of lateral wing retraction and increasing altitude. VALKRIE retracts and extends the wings at the same percentage as a bat, has a wingbeat frequency faster than *Hipposideros diadema*, and can remotely steer to the right and left. While VALKRIE does not match the weight of *Hipposideros diadema*, VALKRIE can overcome the increased weight and still maintain flight.

The wing profile of VALKRIE is the same as that of *Hipposideros diadema* except for the hind legs. Due to the simplification of the hind legs and spine, the hind legs do not have as high a degree of freedom as those of VALKRIE's biological counterpart but compensate by being proportionally larger and having more authority.

VALKRIE's novel simplified wing retraction, mechanical design, and electrical design have allowed VALKRIE to be the first to-scale medium-sized bat-inspired robot to achieve sustained flight.

8.1 Future Work

With the current iteration of VALKRIE, for controls, VALKRIE has a PID for the roll, but VALKRIE also has the potential for a PID for the yaw because the roll and yaw are coupled. The IMU on VALKRIE has a magnetometer that can be used to find the yaw. Regarding trajectory planning for autonomy and straight flying, yaw would be more useful to control than directly controlling the roll. With the ability to estimate pitch, a pitch controller could be implemented to allow for stable flights. With sensor implementation, the camera caused too much of a disturbance on the center of mass. By mounting the sensor at or directly below the center of mass, the camera would be a very viable sensor.

For the many mini-UAV applications, this model can be further researched for autonomy, parameter optimization, complex maneuvering, and attachments of further sensors. With the ability to control pitch and roll and additional data analysis, motion planning and trajectory planning could be incorporated. Many parameters comprise VALKRIE; optimizing these parameters for other bat species could lead to higher efficiency in flight and maneuvering. There is also research into the biology-inspired echolocation of bats; with echolocation, if implemented, VALKRIE would be able to have an understanding of the outside environment. The possibilities for further development of VALKRIE and mini-UAVs are extensive; VALKRIE is a successful baseline for creating an ornithopter capable of being implemented in many different applications and fields.

Sources

[1] Sadier, Alexa, et al. “Making a bat: The developmental basis of bat evolution.” Genetics and molecular biology 43 (2021): e20190146.

[2] Mickleburgh SP, Hutson AM, Racey PA. A review of the global conservation status of bats. Oryx. 2002;36(1):18-34. doi:10.1017/S0030605302000054

[3] Roslan, Azuan. (2014). “Wing Loading and Aspect Ration of Roundleaf Bats” 10.13140/2.1.2952.6085.

[4] “Classification of the Unmanned Aerial Systems.” Classification of the Unmanned Aerial Systems | GEOG 892: Unmanned Aerial Systems, PennState, www.e-education.psu.edu/geog892/node/5#:~:text=4th%20edition%2C%20Wiley-,Small%20UAVs,as%20shown%20in%20Figure%201.2. Accessed 12 Mar. 2024.

[5] Thompson, Avery. “The Flying Batbot Is Seriously Awesome - Popular Mechanics.” Popular Mechanics, www.popularmechanics.com/technology/robots/a19664556/festo-batbot-bionic-flying-fox/. Accessed 29 Jan. 2024.

[6] Ramezani, Alireza, Soon-Jo Chung, and Seth Hutchinson. “A biomimetic robotic platform to study flight specializations of bats.” Science Robotics 2.3 (2017): eaal2505.

[7] “Sensors for Bat-Inspired Spy Plane under Development.” University of Michigan News, 13 Mar. 2008, news.umich.edu/sensors-for-bat-inspired-spy-plane-under-development/. Accessed 29 Jan. 2024.

[8] Colorado, Julian, et al. “Biomechanics of smart wings in a bat robot: morphing wings using SMA actuators.” Bioinspiration & biomimetics 7.3 (2012): 036006.

[9] Hoff, Jonathan, et al. “Bat Bot 2.0: bio-inspired anisotropic skin, passive wrist joints, and redesigned flapping mechanism.” 2021 IEEE/RSJ International Conference on Intelligent Robots and Systems (IROS). IEEE, 2021.

[10] Dai, Junwei, and Handan Wang. “Aerodynamic emulation analysis of bionic bat micro flapping-wing aircraft.” 2022 4th International Conference on Artificial Intelligence and Advanced Manufacturing (AIAM). IEEE, 2022.

[11] Bie, Dawei, et al. “Design, aerodynamic analysis and test flight of a bat-inspired tailless flapping wing unmanned aerial vehicle.” Aerospace Science and Technology 112 (2021): 106557.

[12] Teeling, Emma C., et al. “Bat biology, genomes, and the Bat1K project: to generate chromosome-level genomes for all living bat species.” Annual review of animal biosciences 6 (2018): 23-46.

[13] R/Natureisfuckinglit - I Present to You... the Flying Fox, www.reddit.com/r/NatureIsFuckingLit/comments/7wwm47/i_present_to_you_the_flying_fox/. Accessed 21 Feb. 2024.

[14] Beleno, Jan Vivienel I., and Alma B. Mohagan. “The Diversity and Status of Bats in Quarry Cave, Poblacion, Kitaotao Bukidnon, Philippines.” Asian Journal of Biodiversity 14.1 (2023).

[15] “Khun Kitti Bat: Unveiling the World’s Smallest Mammal; Kitti’s Hog-Nosed Bat " River Kwai Resotel.” River Kwai Resotel, 22 Aug. 2023, www.riverkwairesotel.net/kanchanaburi-blog/worlds-smallest-mammal/.

[16] Bahlman, Joseph W., Sharon M. Swartz, and Kenneth S. Breuer. “How wing kinematics affect power requirements and aerodynamic force production in a robotic bat wing.” Bioinspiration & biomimetics 9.2 (2014): 025008.

[17] Kazilek. “Human, Bird, and Bat Bone Comparison.” Arizona State University, 5 Nov. 2009, askabiologist.asu.edu/human-bird-and-bat-bone-comparison.

[18] Cheney, Jorn A., et al. “Membrane muscle function in the compliant wings of bats.” Bioinspiration & biomimetics 9.2 (2014): 025007.

[19] Witton, Mark P., and Michael B. Habib. “On the size and flight diversity of giant pterosaurs, the use of birds as pterosaur analogues and comments on pterosaur flightlessness.” PloS one 5.11 (2010): e13982.

[20] Song, Arnold, et al. “The aero-mechanics of low aspect ratio compliant membrane wings, with applications to animal flight.” 46th AIAA Aerospace Sciences Meeting and Exhibit. 2008.

[21] Wolf, Marta, et al. “Kinematics of flight and the relationship to the vortex wake of a Pallas' long tongued bat (Glossophaga soricina).” Journal of Experimental Biology 213.12 (2010): 2142-2153.

[22] Furst, Stephen, George Bunget, and Stefan Seelecke. “Design and fabrication of a bat-inspired flapping-flight platform using shape memory alloy muscles and joints.” Smart Materials and Structures 22.1 (2012): 014011.

[23] Alviola, Phillip A., et al. “Dietary analysis of eight insectivorous bats (Chiroptera) from Puting Bato Cave Complex, Burdeos, Polillo Island, Philippines.” Journal of Asia-Pacific Biodiversity 16.3 (2023): 291-299.

[24] Sartore, Joel. “A Diadem Leaf-Nosed Bat (*Hipposideros diadema*) at the University of the Philippines.” Joel Sartore, 12 Sept. 2019, www.joelsartore.com/ani014-00282/. Accessed 27 Jan. 2024.

[25] Kingston, Tigga, et al. “Resource partitioning in rhinolophoid bats revisited.” Oecologia 124 (2000): 332-342.

[26] Bullen, R. D., and N. L. McKenzie. “Scaling bat wingbeat frequency and amplitude.” Journal of experimental biology 205.17 (2002): 2615-2626.

[27] Swartz, Sharon M., and Justine J. Allen. “Structure and Function of Bat Wings.” Phyllostomid Bats: A Unique Mammalian Radiation (2020): 151.

[28] Swartz, Sharon M., et al. “Mechanical properties of bat wing membrane skin.” Journal of Zoology 239.2 (1996): 357-378.

[29] Thollesson, Mikael, and Ulla M. Norberg. “Moments of inertia of bat wings and body.” Journal of Experimental Biology 158.1 (1991): 19-35.

[30] Norberg, Ulla M., et al. “The cost of hovering and forward flight in a nectar-feeding bat, Glossophaga soricina, estimated from aerodynamic theory.” Journal of experimental biology 182.1 (1993): 207-227.

[31] Sekhar, Susheel, et al. “Canonical description of wing kinematics and dynamics for a straight flying insectivorous bat (Hipposideros pratti).” PLoS One 14.6 (2019): e0218672.

[32] “Bambu Lab A1 3D Printer.” Bambu Lab US, us.store.bambulab.com/products/a1. Accessed 22 Feb. 2024.

[33] Ajanic, Enrico, et al. “Robotic avian wing explains aerodynamic advantages of wing folding and stroke tilting in flapping flight.” Advanced Intelligent Systems 5.2 (2023): 2200148.

[34] Merryisha, Samuel, and Parvathy Rajendran. Wing Engineering: Aerodynamics, Structures And Design. Penerbit USM, 2023.

[35] Bergou, Attila J., et al. “Falling with style: bats perform complex aerial rotations by adjusting wing inertia.” PLoS Biology 13.11 (2015): e1002297.

[36] Von Busse, Rhea, et al. “Kinematics and wing shape across flight speed in the bat, Leptonycteris yerbabuenae.” Biology open 1.12 (2012): 1226-1238.

[37] Kitchener, D. J., et al. “Hipposideros diadema (Chiroptera Hipposideridae) in the Lesser Sunda Islands, Indonesia: taxonomy and geographic morphological variation.” Records of the Western Australian Museum 16.1 (1992): 1-60.

[38] “Accessing Accelerometer Data on Nano 33 Ble.” Docs.Arduino.Cc, docs.arduino.cc/tutorials/nano-33-ble/imu-accelerometer/. Accessed 29 Jan. 2024.

[39] Rose, Cameron, and Ronald S. Fearing. “Flight simulation of an ornithopter.” Electrical Engineering and Computer Sciences (2013).